2021

Detrital Neodymium and (Radio)Carbon as Complementary Sedimentary Bedfellows? The Western Arctic Ocean as a Testbed

Melissa S. Schwab

Jörg D. Rickli

Robie W. MacDonald

H. Rodger Harvey
Old Dominion University, rharvey@odu.edu

Negar Haghipour

See next page for additional authors

Original Publication Citation

Schwab, M. S., Rickli, J. D., Macdonald, R. W., Harvey, H. R., Haghipour, N., & Eglinton, T. I. (2021). Detrital neodymium and (radio)carbon as complementary sedimentary bedfellows? The Western Arctic Ocean as a testbed. *Geochimica Et Cosmochimica Acta*, 315, 101-126. https://doi.org/10.1016/j.gca.2021.08.019

Available online at www.sciencedirect.com

ScienceDirect

Geochimica et Cosmochimica Acta 315 (2021) 101–126

Geochimica et Cosmochimica Acta

www.elsevier.com/locate/gca

Detrital neodymium and (radio)carbon as complementary sedimentary bedfellows? The Western Arctic Ocean as a testbed

Melissa S. Schwab [a,*], Jörg D. Rickli [b], Robie W. Macdonald [c], H. Rodger Harvey [d], Negar Haghipour [a,e], Timothy I. Eglinton [a]

[a] *Geological Institute, Department of Earth Sciences, ETH Zurich, Sonneggstrasse 5, 8092 Zurich, Switzerland*
[b] *Institute of Geochemistry and Petrology, Department of Earth Sciences, ETH Zurich, Clausiusstrasse 25, 8092 Zurich, Switzerland*
[c] *Institute of Ocean Sciences, Fisheries and Oceans Canada, 9860 W Saanich Road, Sidney, BC V8L 4B2, Canada*
[d] *Department of Ocean and Earth Sciences, Old Dominion University, Norfolk, VA 23529, USA*
[e] *Laboratory for Ion Beam Physics, Department of Physics, ETH Zurich, Otto-Stern-Weg 5, 8093 Zurich, Switzerland*

Received 6 February 2021; accepted in revised form 18 August 2021; Available online 26 August 2021

Abstract

Interactions between organic and detrital mineral phases strongly influence both the dispersal and accumulation of terrestrial organic carbon (OC) in continental margin sediments. Yet the complex interplay among biological, chemical, and physical processes limits our understanding of how organo-mineral interactions evolve during sediment transfer and burial. In particular, diverse OC sources and complex hydrodynamic processes hinder the assessment of how the partnership of organic matter and its mineral host evolves during supply and dispersal over continental margins. In this study, we integrate new and compiled sedimentological (grain size, surface area), organic (%OC, OC-$\delta^{13}C$, OC-$F^{14}C$), and inorganic isotopic (ε_{Nd}, $^{87}Sr/^{86}Sr$) geochemical data for a broad suite of surface sediments spanning the Western Arctic Ocean from the Bering Sea to the Mackenzie River Delta that capture diverse sources and ages of both terrestrial and marine material deposited in contrasting shelf and slope settings. Spatial gradients in sediment properties were used to delineate regional sources and transport processes influencing the dispersion and persistence of OC-mineral particle associations during export and burial. We found strong relationships between physical parameters, aluminum content, and OC-^{14}C suggesting that terrestrial OC remains tightly associated with its detrital mineral carrier during source-to-sink transport. Notably, carbon and neodymium isotopic data yield consistent information regarding organic matter provenance. Results obtained highlight the potential for coupled organic-inorganic tracer measurements to elucidate sediment sources and to constrain physical and geochemical processes during sediment mobilization and transport in the Western Arctic Ocean. Tandem measurements of carbon and Nd isotopes may provide a new way to identify large-scale biogeochemical and ecological changes in the sources, nature, and fate of OC stemming from predicted increases in sea ice loss and fluvial inputs of dissolved and particulate OC to this complex and dynamic high latitude marginal sea.

Keywords: Western Arctic Ocean; Organic carbon; Carbon-14; Neodymium isotopes; Strontium isotopes; Detrital sediments

* Corresponding author at: Jet Propulsion Laboratory, California Institute of Technology, 4800 Oak Grove Drive, Pasadena, CA 91109, USA.
E-mail address: melissa.s.schwab@jpl.nasa.gov (M.S. Schwab).

https://doi.org/10.1016/j.gca.2021.08.019
0016-7037/

1. INTRODUCTION

1.1. Importance of organo-mineral interactions

Particulate organic carbon (POC) exported from the continents to be dispersed and deposited in continental margin sediments is often closely associated with detrital mineral phases (Burdige, 2005; Blair and Aller, 2012). Such organo-mineral interactions can stabilize organic carbon (OC) by hindering microbial remineralization processes (Keil et al., 1994; Mayer, 1994a; Eusterhues et al., 2003; Burdige, 2007; Mead and Goñi, 2008). These interactions are most pronounced in fine-grained sediments dominated by high mineral surface area (SA) aluminosilicates that protect organic matter (Mayer, 1994a; Hedges and Keil, 1995; Ransom et al., 1998; Galy et al., 2008; Mikutta et al., 2009; Bennett et al., 2012). Stabilization of mineral-hosted organic matter has been attributed to several factors including physical protection by sorption onto mineral surfaces and occlusion within pore spaces (Kaiser and Guggenberger, 2003; Mayer et al., 2004; McCarthy et al., 2008; Mikutta et al., 2009), the formation of microaggregates (Hedges et al., 1997; Bock and Mayer, 2000; Wagai and Mayer, 2007; Curry et al., 2007; McCarthy et al., 2008), and formation of organic-mineral bonds through ion and inner-sphere ligand-exchange reactions (Torn et al., 1997; Kennedy et al., 2002; Kaiser et al., 2007; Kleber et al., 2007). The resultant OC loading (defined as OC/SA) in river and continental margin sediments typically ranges from 0.4 to 1.0 mgC m^{-2} (Mayer, 1994b; Hedges and Keil, 1995; Blair and Aller, 2012).

The intimate association of organic matter with detrital mineral particles may influences its preservation in aquatic environments as well as its hydrodynamic behavior. The propensity for resuspension and lateral transport of fine-grained sediments results in facile mobilization and widespread OC dispersal over continental margins (Wakeham et al., 2009; Hwang et al., 2015; Bao et al., 2016; Wakeham and Canuel, 2016; Tesi et al., 2016; Bao et al., 2018c). As a consequence, organo-mineral interactions appear to exert a fundamental control on the fate of continental-derived OC in the marine realm (Mayer, 1994a; Hedges and Keil, 1995; Blair and Aller, 2012). However, the manner in which these interactions evolve during source-to-sink sediment transfer, and the impact on OC burial patterns and efficiencies remain obscured by the complexity of underlying biological, chemical, and physical processes. Organic carbon deposited in ocean sediments derives from multiple sources and its abundance and composition is the culmination of diverse processes (Hedges et al., 1997; Burdige, 2005; Blair and Aller, 2012; Canuel et al., 2012; Bianchi et al., 2018). Approaches are needed to more fully understand how the partnership between OC and its mineral host evolves during supply and dispersal over continental margins.

The radiocarbon and stable carbon isotopic composition of OC have been valuable metrics to discriminate between terrestrial and marine organic matter contributions to sediments (e.g., Goñi et al., 2005; Mead and Goñi, 2008; Wakeham et al., 2009; Vonk et al., 2010; Goñi et al., 2013; Vonk et al., 2015; Bao et al., 2018c), with ^{14}C-, and ^{13}C-depleted values generally attributed to the supply of pre-aged, C_3 higher plant-derived organic matter from the continents. When combined with OC loadings, carbon isotopic information has been used to assess the burial efficiency of terrestrial OC in marine sediments (e.g., Burdige, 2005; Burdige, 2007; Rothman and Forney, 2007). Radiogenic Nd and Sr isotopic compositions are commonly used as tracers of inorganic sediment provenance and to track source regions and transport pathways of detrital mineral particles (e.g., Hwang et al., 2021). Although Sr isotopic ratios can deviate from their source rock values as a result of mineral sorting during transport (Meyer et al., 2011; Garçon et al., 2014; Jonell et al., 2018), Nd isotopic compositions are largely unaffected by weathering, transport, or deposition, and reflect the original composition of their source rocks (Garçon et al., 2013; Bayon et al., 2015). The linking of Nd and carbon isotopic compositions may, hence, help constraining both sources of OC and its mineral host, as well as the extent to which these components remain coupled during transport and deposition on continental margins.

1.2. The Western Arctic as a natural laboratory

Strong isotopic contrasts among putative source regions are a necessary prerequisite for the application of a combined organic and inorganic isotopic tracer approach. Landmasses surrounding the Western Arctic Ocean exhibit pronounced environmental and geological contrasts which makes it a valuable testbed. Watersheds draining into the Western Arctic Ocean contain extensive tracts of permafrost and host vast quantities of pre-aged, ^{13}C-depleted, terrestrial OC. Associated lithogenic material eroding from these landscapes is exported to Arctic marginal seas, where it is intermixed with OC derived from modern marine primary productivity (Goñi et al., 2005; Goñi et al., 2013; Schreiner et al., 2013; Vonk et al., 2015). This mixing manifests itself in sharp contrasts in the ^{14}C age of OC derived from marine and terrestrial sources (Griffith et al., 2012; Druffel et al., 2017). Given the large variations in geologic age and bedrock type, detrital sediments eroded from these various source regions (Canadian Shield, Siberian magmatic provinces, North American Cordillera in Alaska, and Aleutian volcanic arc) exhibit marked differences in Nd and Sr isotopic signatures (Asahara et al., 2012; Schreiner et al., 2013; Maccali et al., 2018).

In this study, we exploit strong isotopic gradients that exist within the Western Arctic region to constrain the provenance of terrestrial organic matter and detrital minerals deposited in this high latitude continental margin system. We present physical (grain size, SA), organic (%OC, OC-$\delta^{13}C$, OC-$F^{14}C$), and inorganic (ε_{Nd}, $^{87}Sr/^{86}Sr$) geochemical characteristics of surface sediments. These new measurements are combined with previously published data to develop a comprehensive spatial analysis of modern-day transport processes and pathways that influence the fate of terrestrial organic and detrital matter. The observations provide a benchmark for assessing past

and future changes in the supply of marine and terrigenous material, as well as in the associated hydrographic conditions and depositional environments.

2. ENVIRONMENTAL SETTING

2.1. Regional physiography and ocean circulation

As a result of its semi-enclosed nature that restricts water circulation, the Arctic Ocean is commonly referred to as high latitude "Mediterranean Sea" (e.g., Aagaard and Carmack, 1989; Stein and Macdonald, 2004). Another unique geomorphological feature is the extensive shallow shelf region encompassing more than half of the total oceanic area (52.9%; Jakobsson et al., 2003; Jakobsson et al., 2012). The northern Bering and the Chukchi Sea, located on broad and shallow shelves with average depths of 50 m (Fig. 1), are regarded as inflow shelves (Carmack et al., 2006; Macdonald et al., 2015), providing about a third of the total water input to the Arctic Ocean (Woodgate and Aagaard, 2005). Pacific water entering through the shallow (ca. 54 m) and narrow (ca. 85 km) Bering Strait varies seasonally and interannually in temperature, salinity, and nutrient content (Coachman et al., 1975; Weingartner et al., 2005; Woodgate et al., 2005; Danielson et al., 2017). The cold, salty, and nutrient-rich Anadyr Current flows northward along the Kamchatkan coast. On the opposite side of the Bering Strait, the Alaskan Coastal Current, mainly fed by fluvial runoff into the Gulf of Alaska (Corlett and Pickart, 2017), delivers warmer, nutrient-depleted waters to the Chukchi Sea. Bering Shelf waters are characterized by intermediate temperature and salinity (Stabeno et al., 2018). Upon entering the Chukchi Sea, Anadyr and central Bering Shelf water bodies mix and form Bering Shelf-Anadyr Water (Grebmeier et al., 1988; Grebmeier et al., 2006).

Submerged ridges and shoals force water traversing the Chukchi Shelf to branch, breaking into three distinct pathways (Fig. 1, Coachman et al., 1975; Weingartner et al., 2005). The western pathway steers Pacific water between Wrangel Island and Herald Shoal towards Herald Canyon. The eastern pathway proceeds along the Alaskan coastline and exits through Barrow Canyon. Waters following the Central Channel bifurcate around Hanna Shoal and ultimately enter Barrow Canyon (Pickart et al., 2016). Portions of Pacific-origin water advected through Herald and

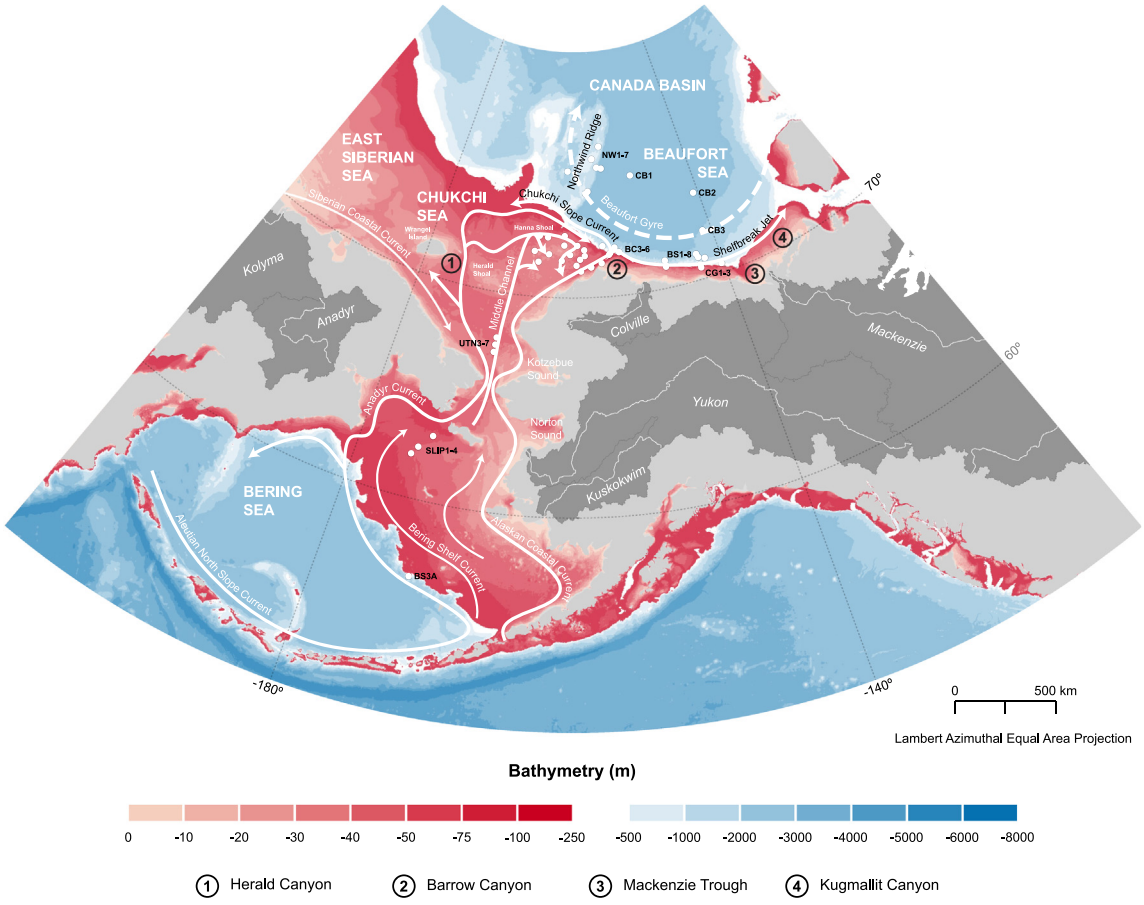

Fig. 1. Map of the Western Arctic Ocean depicting ocean circulation patterns as well as the main river systems. Surface sediment sample locations are indicated as white dots. Dark grey areas represent major river drainage basins. The locations of Herald Canyon, Barrow Canyon, the Mackenzie Trough, and Kugmallit Canyon are indicated by circled numbers (1–4, respectively). Schematic circulation in the Western Arctic Ocean is adapted from Corlett and Pickart (2017).

Barrow Canyons form eastward-directed shelfbreak jets along the edge of the Chukchi and Beaufort Seas (Pickart, 2004; Nikolopoulos et al., 2009; Corlett and Pickart, 2017; Li et al., 2019). However, the majority of Pacific water emanating from Barrow Canyon is transported westwards above the upper continental slope as Chukchi Slope Current (Corlett and Pickart, 2017; Stabeno et al., 2018; Li et al., 2019).

Contrasting sharply with the extensive shelf area of the Bering and Chukchi Seas, the Beaufort Shelf - extending along the Alaskan and Canadian coasts - is characterized by a narrow and steep margin descending into the Canada Basin (max. depth ca. 3800 m). The Canada Basin is bordered to the west by the 500 km long and 100 km wide Northwind Ridge. In particular, the eastern flank of the Northwind Ridge sharply rises to 3400 m above the Canada Abyssal Plan forming an escarpment. Pacific water exiting Barrow Canyon is transported eastward by the Beaufort undercurrent where it promotes eddies and downwelling along the shelfbreak (D'Asaro, 1988; Pickart, 2004). However, the dominant surface currents within the Canada Basin and the Beaufort Sea are dictated by the anticyclonic Beaufort Gyre where winds drive surface water and sea-ice westward in a clockwise motion.

2.2. Surrounding geology

The geology surrounding the Western Arctic Ocean is complex, but it can be described broadly in terms of four main units (Fig. S1 a), namely orogenic fold belts, magmatic provinces, sedimentary platforms, and Archean shields (Dürr et al., 2005; Hartmann and Moosdorf, 2012).

The North American Cordillera is part of the Circum-Pacific orogenic belt dominated by accretionary tectonics. The Cordilleran system encompasses sedimentary and metamorphic rocks as well as the Cordilleran magmatic arc built along the active continental margin (Dickinson, 2004). Volcanism is also expressed in the Okhotsk-Chukotka and the Bering Sea basalt provinces. Further volcanic activity occurs along the convergent margins of the Pacific Aleutian and the Koryak-Kamchatka Arcs. Sedimentary provinces in Northern America, in particular the Interior Platform including the Western Plain of Alberta and British Columbia, consist of undeformed and uncompacted marine shales, black shales, sandstones, and limestones of Cambrian to Cretaceous age (Millot et al., 2003). Precambrian basement outcrops in the Slave Province (Canadian Shield), the North American Cordillera, and in Chukotka.

The contrasting felsic and mafic lithologies surrounding the Western Arctic, and their variable ages, lead to strong contrasts in radiogenic signatures of the sediments sourced from these regions (Fig. S1 b and c). This variability is exploited here to constrain sources of terrestrial sediments and associated OC (see Sections 4.3, 5.2, 5.5).

2.3. Sediment sources and accumulation rates

Although the Arctic Ocean constitutes only ~1% of the global ocean volume, it receives ~11% of the global river water and associated sediment discharge (Aagaard and Carmack, 1989; McClelland et al., 2012). The Mackenzie River supplies up to 128 Mt yr^{-1} of sediment (Carson et al., 1998; Carson et al., 1999) and 1.8–2.2 TgC yr^{-1} of POC (Goñi et al., 2000; McGuire et al., 2009; Hilton et al., 2015) to the Beaufort Shelf rendering it the single largest point source of particulate matter to the Arctic Ocean (Holmes, 2002). The majority of the particulate matter stems from erosion of surface soils in the North American Cordillera delivered by streams and rivers (Carson et al., 1998; Yunker et al., 2002). The Alaskan Colville River originating in the Cordillera Mountains is situated exclusively in continuous permafrost. The total sediment flux of the Colville River is estimated at 5.8 Mt yr^{-1} (Arnborg et al, 1967). Due to protracted storage in permafrost soils and floodplains, the POC transferred by the Mackenzie and Colville Rivers is highly degraded and extensively pre-aged upon discharge to the Beaufort Shelf (Yunker and Macdonald, 1995; Goñi et al., 2000; Schreiner et al., 2013; Feng et al., 2013; Hilton et al., 2015; Vonk et al., 2015; Zhang et al., 2017; Vonk et al., 2019; Schwab et al., 2020). Although dominated by riverine inputs, the Beaufort Shelf also receives minor sedimentary contribution through coastal erosion (sediment ~8 Mt yr^{-1}, 0.1 MgC yr^{-1}; e.g., Grigoriev et al., 2004; Jorgenson and Brown, 2005).

The dominant terrestrial sources of sediment to the Bering Sea are the Yukon and the Kuskokwim Rivers, draining the Alaskan mainland, and the Anadyr River draining northeastern Siberia. Annual sediment loads amount to 54, 8, and 2 Mt yr^{-1}, respectively (VanLaningham et al., 2009; Milliman and Farnsworth, 2011). The annual sediment input from eroding shorelines reaches 70 Mt yr^{-1} (0.8 MgC yr^{-1}) in the Chukchi Sea (Grigoriev et al., 2004) and 20 Mt yr^{-1} in the Bering Sea (VanLaningham et al., 2009).

The northern Bering and southern Chukchi Shelves rank among the most productive areas in the world's oceans. Nutrient-rich Pacific water promotes primary productivity on the Bering and Chukchi Shelves averaging to 470 gC m^{-2} yr^{-1} (Sakshaug, 2004; Hill and Cota, 2005; Arrigo and van Dijken, 2015). Shallow water columns restrict remineralization during sinking and allow the accumulation of organic-rich sediments (Grebmeier and Cooper, 1995; Grebmeier et al., 2006) supporting abundant benthic communities (Dunton et al., 2005; Grebmeier et al., 2006; Kuzyk et al., 2013). In particular, the upwelling at the head of Barrow Canyon promotes phytoplankton blooms (Hill and Cota, 2005; Cooper et al., 2009; Pisareva et al., 2019), while deeper canyon regions are characterized by off-shore particle transport and deposition (Goñi et al., 2013; Kuzyk et al., 2013). In contrast, primary productivity on the Beaufort Shelf is considered oligotrophic (30–70 gC m^{-2} yr^{-1}; Sakshaug, 2004; Carmack et al., 2006).

The highest sediment accumulation rates are observed in the Bering and Chukchi Seas ranging from 0.13 to 0.44 g cm^{-2} yr^{-1} (Asahara et al., 2012; Oguri et al., 2012; Kuzyk et al., 2017). Accumulation rates in the Barrow Canyon and Beaufort Sea display intermediate values from 0.04 to 0.18 g cm^{-2} yr^{-1} (Kuzyk et al., 2017) whereas the

open Canada Basin is regarded as sediment starved (Grantz et al., 1996; Schneider et al., 1996; Backman et al., 2004; Hwang et al., 2015).

3. METHODS

3.1. Sample collection

The sediment core repository at the Woods Hole Oceanographic Institution (WHOI) provided nineteen core-top samples (0–2 cm) from undisturbed multi and box cores as well as from two giant gravity cores. The cores were collected during cruises in 1989, 1992, and 1993 aboard the USCGC *Polarstar* (Grantz et al., 1994), and aboard the USCGC *Healy* in 2002. These samples were collected from the Northwind Ridge (NWR-1 to 7, Fig. 1, Table S1), the Beaufort Shelf (BS-1 to 8), and the Canada Basin (CB-1 to 3). The core-top sediments supplied by WHOI were not frozen during storage. Hence, they were not suitable for the analyses of organic carbon isotopes, which were omitted. In contrast to carbon isotopes, radiogenic Nd and Sr isotopic compositions are not susceptible to alteration during storage at ambient temperature which allowed measurements of radiogenic Nd and Sr signatures in detrital sedimentary fractions for this study (see Section 3.4). Storage at ambient temperature may influence the reactivity of non-detrital sedimentary fractions, potentially affecting the leaching experiments (see Section 3.5). Such effects have, to our knowledge, not been studied in detail.

Fourteen core-top samples were retrieved aboard the CCGS *Sir Wilfrid Laurier* in July 2007 as part of the Canadian International Polar Year (Pouliot box-corer) comprising sampling locations in the Bering Sea (BS3A, SLIP-1,3,4), the Chukchi Sea (UTN-3,5,7), the Barrow Canyon (BC-3,4,5,6), and on the Beaufort Sea Slope (CG-1,2,3). Detailed characteristics of locations and subsampling methods were published in previous studies (Macdonald and Gobeil, 2012; Goñi et al., 2013; Kuzyk et al., 2013, 2017). Further surface sediment samples from the Chukchi Sea (n = 18) were obtained during the Chukchi Offshore Monitoring in Drilling Area – Hanna Shoal (COMIDA HS) in 2012 and 2013 aboard the USCGS *Healy* (Belicka and Harvey, 2009; Dunton et al., 2017; Harvey and Taylor, 2017).

3.2. Sedimentological analyses

Subsamples for grain size and SA measurements were thermally oxidized to remove OC (450°C, 6 h). Sedimentary material for grain size distribution measurements (0.02–2000 μm) was dispersed in a 5 g L^{-1}Na-polyphosphate dispersion agent and subsequently analyzed using a Malvern Mastersizer 2000 laser diffraction granulometer (Malvern Instruments Ltd) coupled to a Hydro 2000S ultrasonic dispersion unit (Geological Institute, ETH Zurich). Analytical reproducibility was estimated to be 10% based on the relative standard deviation of the modal size of repeated sample measurements. Statistical parameters (e.g., mean, sorting) were calculated following Folk and Ward (1957) using GRADISTATv8 (Blott and Pye, 2001).

Surface area analysis was performed on a NOVA 4000e Surface Area Analyzer (Geological Institute, ETH Zurich). Degassed samples (350°C, 8 h; Quantachrome FLOVAC degasser) were analyzed using the Quantachrome NovaWin software generating a 5-point BET method (Mayer, 1994b; Keil et al., 1997). Empirical correlation coefficients were > 0.9998 for all samples.

3.3. Elemental and isotopic analyses of carbon

About 60 mg (equivalent to ~0.9–1.0 mg C) of sediment was placed in Ag capsules and treated with acid vapor (70°C, 72 h) to remove inorganic carbon (Bao et al., 2018a, 2018b, 2018c). After neutralization with NaOH (70°C, 72 h) samples were wrapped in tin boats. Graphitization of the sediments was performed using an elemental analyzer-automated graphitization system (Wacker et al., 2010). Absolute concentrations and ^{13}C isotopic content (‰VPDB) of de-carbonated samples were measured with an elemental analyzer-isotope ratio mass spectrometer (EA-IRMS, Elementar, Vario MICRO cube – Isoprime, Vison). Based on peptone (Sigma) and atropine (Säntis) standards, accuracy of OC contents and OC-$\delta^{13}C$ corresponded to values better than 0.03% and 0.1‰. The ^{14}C content of graphite targets was measured on a mini carbon dating system (MICADAS) at the Laboratory of Ion Beam Physics, ETH Zurich (Wacker et al., 2010). Samples were calibrated against oxalic acid II (NIST SRM 4990C; precision of 1‰), phthalic acid, and an in-house anthracite coal blank. Reported ^{14}C data are expressed as $F^{14}C$ values (Reimer et al., 2004).

3.4. Trace element and radiogenic isotope analyses of detrital fractions

The detrital fraction, which records information on the continental sources of sediments, was isolated for inorganic geochemical analysis following sequential extraction procedures described in Bayon et al. (2002). In brief, carbonate and ferromanganese (FeMn) oxides, potentially of mixed marine and terrestrial origin, were removed consecutively by adding 10 mL of 10% acetic acid (room temperature, 4 h) and 10 mL of 1 M hydroxylamine hydrochloride in 25% acetic acid (90°C, 3 h), respectively. The residual silicate fraction was digested in a 4:1 mixture of 28 M HF and 14.5 M HNO_3. In preparation for column chemistry, the digested detrital fraction was treated twice in 3 mL concentrated HNO_3 and 200 μL hydrogen peroxide to oxidize OC. A small aliquot of sample stock solutions was used for concentration measurements of Sr, Al, and Fe by Inductively Coupled Plasma Mass Spectrometry (ICP-MS) at ETH Zurich (Thermo Scientific Element XR). Sample signals were corrected for machine background corresponding to <1%. Reported bulk concentrations refer to the mass of an element found in the detrital fraction per weighed bulk sample, meanwhile, detrital concentrations are reported relative to the weighed detrital mass after leaching. Precision and accuracy were

assessed through repeated measurements of secondary standards during the four measuring sessions, including river standard SLRS5 (National Research Council of Canada) and the shale standard SGR1 (USGS). The deviation of average measured concentrations from certified values ranged between 0 and 11%, with precisions between 3 and 5% (1 SD). Nd concentrations were calculated using isotope dilution during isotope measurements and have uncertainties <1% (1 SD).

For Nd and Sr isotope measurements, aliquots of sample stock solutions were spiked with an appropriate amount of ^{150}Nd. Rb and Sr were chemically separated from rare earth elements (REEs, including Nd) using a standard cation exchange column (1 mL resin bed, AG50W-X8). Nd was separated from other REEs on Ln Spec resin (Pin et al., 1997), while Sr was separated from Rb on Sr Spec resin (Deniel and Pin, 2001). Isotopic compositions of Nd and Sr were measured using a Thermo Scientific Neptune Plus MC-ICP-MS at ETH Zurich. Total chemical blanks for Sr and Nd corresponded to <9 pg and <11 pg (n = 4), including digestion in HF and HNO_3 and column chemistry. Blanks were insignificant compared to sample sizes >100 ng. Instrumental mass bias correction followed Vance and Thirlwall (2002) in the case of Nd and used a natural $^{86}Sr/^{88}Sr$ ratio of 0.11940 for Sr. External reproducibility of the mass spectrometric analysis was monitored in each session by repeated measurements of La Jolla for Nd and NIST 987 for Sr and corresponds to <13 ppm for $^{143}Nd/^{144}Nd$ and <26 ppm for $^{87}Sr/^{86}Sr$ (2 SD, n ≥ 15 in all sessions). All sample data are normalized to the corresponding literature value of 0.511856 for La Jolla and 0.710248 for NIST 987 (Thirlwall, 1991). Three full replicates of two rock standards, BCR-2 and AGV-2, yielded an error of 13 ppm for Nd (n = 6, 2 SD) and of 81 ppm for Sr isotope compositions (n = 6, 2 SD). Neodymium isotope ratios of the analyzed sediments are expressed in epsilon-notation as relative deviations from the bulk silicate earth ($^{143}Nd/^{144}Nd = 0.512638$; Jacobsen and Wasserburg, 1980).

To account for variability in sediment accumulation rates, coring method, sample availability, and leaching reproducibility, we performed duplicate analyses on sediment aliquots from a range of cores. Six duplicates reflected different depths within the topmost 2 cm, three duplicates included an extra step to remove OC, and two duplicates are full duplicates (same core and depth, same performed leaching steps). Some of these duplicates agreed in their ε_{Nd} within the uncertainty reported for the analyzed rock standards. In other cases, the differences were, however, much larger - up to 0.003 for Sr isotopes and up to 1.2 ε_{Nd}. Based on the variable reproducibility, it seems likely that some of the sediment cores were isotopically more heterogeneous than others. As a result, it is non-trivial to estimate a general uncertainty for the isotope measurements. Nonetheless, the uncertainty (1 SD) of ±0.0006 for Sr isotopes and ±0.37 ε_{Nd}-units estimated using all duplicates, is small compared to the variability among samples collected across the study area ranging between 0.707 and 0.730 in $^{87}Sr/^{86}Sr$ and between −15 and −3.9 in ε_{Nd}.

3.5. Sr and Nd isotope compositions and concentrations of leached fractions

In addition to detrital phase measurements, we selected five surface samples (SLIP4, UTN7, H27, BC3, GC3) characterized by a range of OC contents for measurement of Sr and Nd concentrations and isotopic compositions of carbonate, FeMn, and organic fractions. The carbonate and FeMn oxide fractions were obtained as described in Section 3.4. Organic carbon was subsequently leached at 85°C for 5 h with 10 mL of a 3:5 mixture of 0.02 M HNO_3 and 30% H_2O_2 adjusted to pH 2 (Tessier et al., 1979). The residual silicate fraction was digested in a 4:1 mixture of 28 M HF and 14.5 M HNO_3. Neodymium and Sr isotopic composition and elemental concentrations of these leachates were determined as detailed in Section 3.4 for the detrital fractions.

3.6. Data analysis

3.6.1. General data analysis

To account for the non-normal character of sedimentological and geochemical parameters, we applied the Spearman rank-order correlation coefficient (r_S, significant for $p < 0.05$). All statistical analyses were performed using the open-source statistical software R 4.0.4 (R Core Team, 2020).

3.6.2. Geostatistical interpolation

Inverse distance weighted (IDW) interpolation was used to produce inclusive and comprehensive maps describing the distribution of sedimentary and geochemical parameters in the Western Arctic Ocean. The IDW approach assumes that the attributed value of an unknown point is the weighted average of known values within its neighborhood. Weights are inversely related to the distances between the predicted and sampled locations. More specifically, the isotopic composition z at an unobserved location x is a weighted mean of nearby observations,

$$z(x) = \frac{\sum_i^n w_i z_i}{\sum_i^n w_i} \quad (1)$$

with weights w_i

$$w_i = |x - x_i|^{-\beta} \quad (2)$$

applying the inverse distance power $\beta \geq 0$. We used leave-one-out cross-validation (LOOCV) to estimate the best fit for β and the number of nearest neighbors. Best fit parameters are listed in Table S2 and model residuals are visualized in Fig. S2, S3, and S4. Several add-on R packages were used for fitting IDW models, in particular gstat (Pebesma and Graeler, 2020).

3.6.3. Constraining marine and terrigenous inputs of organic carbon

A Bayesian dual mixing model implemented in the R package simmr (Parnell et al., 2010; Parnell et al., 2013) was applied to estimate relative source contributions of marine and terrigenous OC of surface sediments. We based the isotope mass balance on observed OC-$\delta^{13}C$ and

OC-$F^{14}C$ (see below). The model was fitted with a Markov chain Monte Carlo algorithm that repeatedly projected plausible solutions for each potential source for every sediment sample. Model fitting was carried out by *Just Another Gibbs Sampler* code (Parnell et al., 2013). Uncertainties, residuals, and process errors were propagated throughout the model. The model used default settings while excluding trophic enrichment factors and preferential source contributions.

The isotopic compositions of the marine and terrestrial source end-members were derived from published organic matter signatures for the Western Arctic Ocean and surrounding landmass. In order to establish a common terrestrial end-member accounting for the OC delivered from both inland and coastal sources, we combined suspended river and peat material. First, we calculated mean and SD for each specific source (see Table 1). We then computed a flux weighted mean using the annual sediment flux of each river and of coastal erosion. The resulting OC-$\delta^{13}C$ and OC-$F^{14}C$ of the terrestrial end-member correspond to -27.58 ± 1.08‰ (based on n = 871 actual observations) and 0.55 ± 0.16 (n = 603).

The OC-$\delta^{13}C$ of the marine OC end-member relied on the OC-$\delta^{13}C$ compositions of phytoplankton and ice algae. Marine OC-$\delta^{13}C$ values were often reported as ranges due to the seasonal impacts of ice cover on dissolved inorganic carbon (DIC). We applied Monte Carlo simulations to constrain the uncertainties of the marine end-member composition resulting in an OC-$\delta^{13}C$ value of -20.74 ± 2.01‰. Due to a lack of OC-$F^{14}C$ measurements on plankton-OC we adapted an OC-$F^{14}C$ value of 1.02 ± 0.02 (n = 34) based on DIC in the photic zone (0–200 m) of the Western Arctic Ocean (Griffith et al., 2012; Druffel et al., 2017).

4. RESULTS

4.1. Distribution of sedimentological properties

The mean sediment grain size (Table S1) of surface samples ranges from very fine (M_G = 3.1 μm) to coarse silt (M_G = 27.4 μm), with the exception of sample BS3A from the southern Bering Sea, which corresponds to very fine sand (M_G = 141.1 μm). Sediment samples are poorly to very poorly sorted ($2.3 < \sigma_G < 5.8$). The clay fraction in the non-deltaic Bering and Chukchi Seas sediments including Barrow Canyon is typically below 16%, while deep water and deltaic sedimentary settings in the Beaufort Sea, the Canada Basin, and on the Northwind Ridge are enriched in clay (14–37%; Fig. 2 a, Fig. S5). Elevated fine silt is observed on the Beaufort Shelf and in the Canada Basin. The proportions of fine, medium, and coarse silt are similar in the Bering Sea, the Chukchi Sea, and the Barrow Canyon, corresponding to ca. 30, 23, and 25% respectively. The majority of the investigated samples contain <10% of sandy material. However, sand is locally significant in the Bering (BS3A), the Chukchi (H24, H34, UTN3), and the Beaufort Seas (BS8).

Bulk sediment SA (Table S1) ranges from 4.9 to 37.7 $m^2\ g^{-1}$ and is positively correlated with the proportion of clay (r_S = 0.73, n = 55, $p < 0.001$). Higher SA values (SA > 30 $m^2\ g^{-1}$) occur in the Beaufort Sea, the Canada Basin, and on the Northwind Ridge, which receive higher amounts of fine-grained material. Mean SA in the Bering and Chukchi Seas, as well as the Barrow Canyon, varies from 17.4 to 25.9 $m^2\ g^{-1}$. Clear trends are not evident with water depth or spatial distribution. Observed Al contents range from 3.7 (BC3) to 9.0 wt% (CG3), averaging 6.2 ± 1.2 wt% (Table S3).

4.2. Bulk organic carbon composition

In general, the OC content of the analyzed sediments varies between 1 and 2 wt% along the Western Arctic margin (Fig. 2 b and Fig. 3, Table S3). The lowest values occur in the sandy matrix of the southern Bering Sea (BS3A, 0.28 wt%), the highest in the southern Chukchi Sea (UTN7, 2.56 wt%) and at the shallowest station within the Barrow Canyon (BC3, 4.73 wt%). In combination with previous data (see references in Table S4), POC contents in surface sediments display a strong positive correlation ($r_S = 0.75$, n = 2091, $p < 0.001$) with the sum of silt and clay fractions (Fig. 3; Grebmeier and Cooper, 1995; Grebmeier et al., 2006). In contrast, the statistical relationship between POC content and SA is less pronounced ($r_S = 0.35$, n = 65, $p = 0.004$) (Goñi et al., 2013; Li et al., 2017), and similar to the correlations between POC and Al ($r_S = 0.20$, n = 224, $p = 0.002$) as well as Fe ($r_S = 0.14$, n = 227, $p = 0.04$).

Bulk sediment OC-$\delta^{13}C$ values across the Western Arctic Ocean range from −25.1 to −20.6‰, consistent with those from previous studies (Fig. 4 a, Table S3) (e.g., Naidu et al., 1993, 2000; Stein and Macdonald, 2004; Grebmeier et al., 2006; Cooper et al., 2009; Griffith et al., 2012). The spatial pattern reveals lower $\delta^{13}C$ values close to the Anadyr, Colville, Mackenzie, and Yukon River mouths (<-25‰), and within the Barrow Canyon suggesting enhanced contributions from ^{13}C-depleted, terrigenous organic matter (McMahon et al., 2021). In contrast, open shelf regions of the Bering and Chukchi Seas are relatively enriched in ^{13}C, reflecting the distance from continental sources and increased proportions of OC derived from marine primary productivity.

The OC-$F^{14}C$ composition of surface sediments is highly variable (Fig. 4 b, Table S3). While OC-$F^{14}C$ signatures in the Bering and Chukchi Seas show values ranging from 0.57 to 0.83, the Beaufort Sea and Barrow Canyon are characterized by lower OC-$F^{14}C$ values, varying from 0.37 to 0.46. In comparison, the sediment sample collected from the Barrow Canyon head is markedly enriched in ^{14}C (OC-$F^{14}C$ = 0.86) suggesting an enhanced contribution of marine primary productivity.

4.3. Neodymium and strontium concentrations and isotopic compositions

4.3.1. Detrital fraction

The Nd concentrations of detrital sediment fractions vary from 8.5 to 30.3 ppm (Table S3) and delineate a clear decrease from the Canada Basin to the Bering Sea. The highest detrital Sr concentrations are found in the Bering

Table 1
Compilation of organic carbon, Nd, and Sr isotopic values in Arctic rivers, vegetation, peat, marine primary producers, kerogen, and bedrock. Sources: (1) Holmes (2002); (2) (Schwab et al., 2020); (3) McClelland et al. (2016); (4) Hilton et al. (2015); (5) Naidu et al. (2000); (6) Goñi et al. (2005); (7) Guo et al. (2007); (8) Vonk et al. (2015); (9) Campeau et al. (2020); (10) Goldstein et al. (1984); (11) Millot et al. (2003); (12) Zimmermann et al. (2009); (13) Schreiner et al. (2013); (14) Guo and Macdonald (2006); (15) Asahara et al. (2012); (16) VanLaningham et al. (2009); (17) Schell (1983); (18) Kielland and Bryant (1998); (19) Norris et al. (2016); (20) Preston et al. (2006); (21) Ruttenberg and Goñi (1997); (22) Lawrence et al. (2020); (23) Oelbermann et al. (2008); (24) Xu et al. (2009); (25) Stein and Macdonald (2004); (26) Griffith et al. (2012); (27) Druffel et al. (2017); (28) Hobson et al. (1995); (29) Fischer (1991); (30) Schubert and Calvert (2001); (31) Lewan (1986); (32) (GEOROC, 2021).

Source	Sediment flux (Mt/yr)	n	POC - $\delta^{13}C$ (‰) ± SD	n	POC-$F^{14}C$ ± SD	n	ε_{Nd} ± SD	n	$^{87}Sr/^{86}Sr$ ± SD	Ref.
Suspended sediments										
Mackenzie River	128	123	−27.40 ± 1.46	87	0.41 ± 0.08	9	−12.91 ± 0.84	3	0.731 ± 0.004	1–12
Colville River	5.8	4	−26.78 ± 0.22		0.38	2	−5.40 ± 0.08	2	0.717 ± 0.003	1,5, 12, 13
Yukon River	60	65	−29.06 ± 3.39	12	0.59 ± 0.09	3	−8.58 ± 0.76		0.709	1,3, 7–8, 14–16
Kolyma River	10.1	59	−29.84 ± 2.39	30	0.59 ± 0.10					1,3
Anadyr River	2	5	−26.16 ± 0.49				−2.00		0.735	5, 16
Terrestrial vegetation		70	−27.41 ± 1.09	est.	1.00 ± 0.01					17–20
Permafrost soil	78[a]	615	−26.56 ± 1.68	474	0.74 ± 0.32				0.727	7, 17, 21–25
Marine phytoplankton		est.	−21.50 ± 3.50	34	1.01 ± 0.02					25–27
Ice algae		est.	−20.00 ± 2.00	34	1.01 ± 0.02					25–30
Kerogen		58	−27.55 ± 2.73	est.	0.00 ± 0.01					31
Bed rock										
Aleutian Arc						480	6.4 ± 4.6	695	0.704 ± 0.001	32
Arctic-Alaska-Chukotka						6	−6.9 ± 2.6			32
Bering Sea Basalt Province						28	3.6 ± 6.0	30	0.704 ± 0.003	32
Canadian Shield						170	−9.5 ± 6.3	151	0.707 ± 0.002	32
Kamchatka Arc						594	8.0 ± 2.8	636	0.704 ± 0.001	32
Mackenzie Large Igneous Province						97	−8.1 ± 7.8	10	0.712 ± 0.006	32
North American Cordillera						355	3.7 ± 4.8	108	0.707 ± 0.015	32
Okhotsk-Chukotka Arc						87	−0.9 ± 5.5	95	0.710 ± 0.010	32
Slave Province						113	−14.3 ± 16.6	2	0.703 ± 0.003	32

[a] Annual erosion rates include only Chukchi and Beaufort Seas.

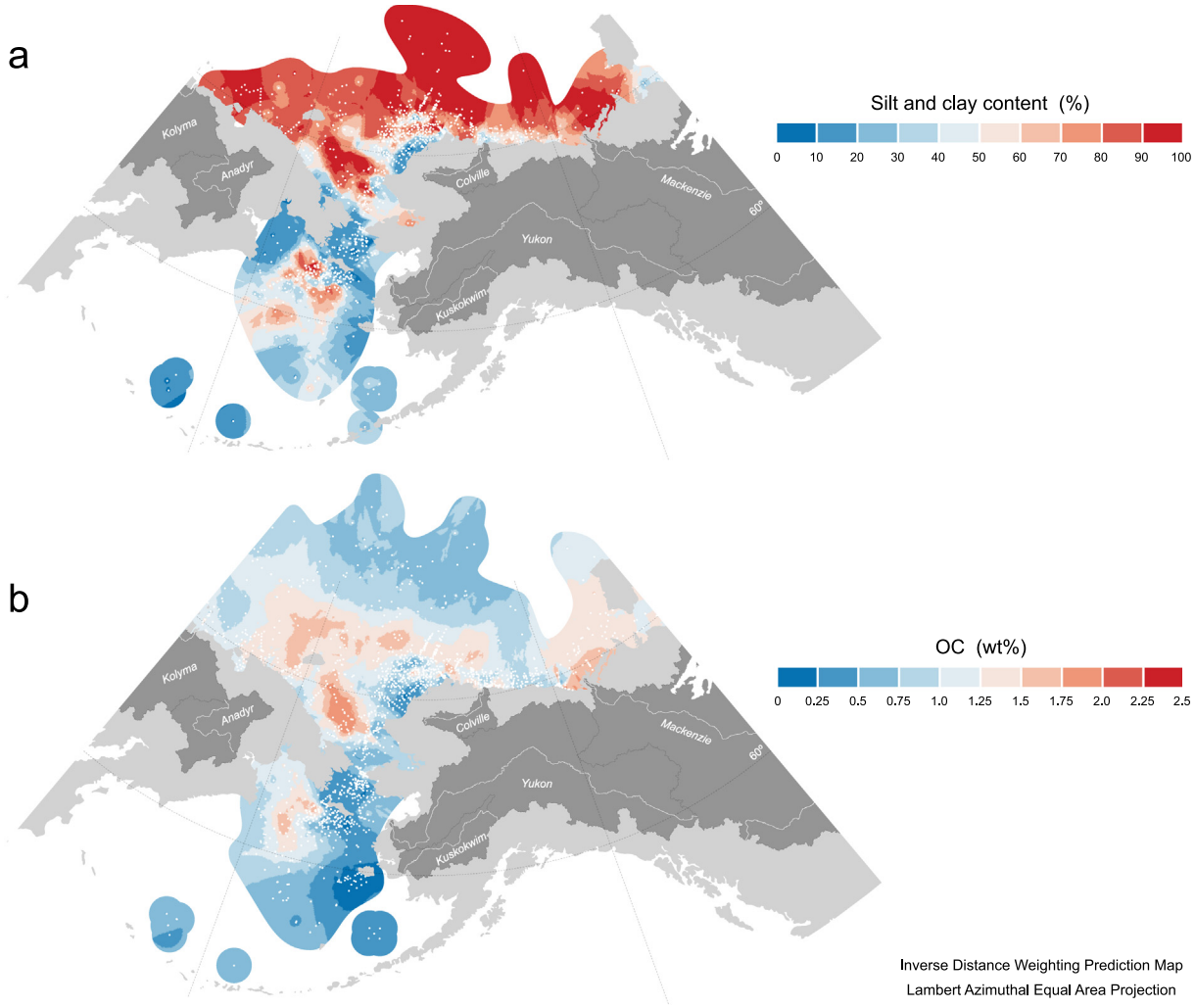

Fig. 2. Spatial distribution maps of (a) summed silt and clay content (%; n = 2257) and (b) organic carbon content (OC, wt%; n = 2935). Maps produced using inverse distance weighting prediction. White dots represent all available observations, including literature data and data from this study. References for published values are listed in Table S4. Dark grey areas represent major river drainage basins.

Sea (274.9 ppm) and the lowest in the northern Chukchi Sea (47.4 ppm). The distributions of both Nd and Sr isotopic compositions show similar east-west trends (Fig. 5). Neodymium isotope compositions range from −15.0 in the Beaufort Sea to −3.9 in the Bering Sea. Strontium isotopic compositions display a more continuous spatial gradient, with the least radiogenic signatures (lowest values) observed in the Bering Sea (0.707) and the most radiogenic signatures located in the Beaufort Sea (0.729).

4.3.2. Leached fractions

Data for measured non-detrital fractions are shown in Fig. 6 and Table S5. The carbonate and FeMn fractions contain 7.6–11.3% and 7.3–16.6% of the bulk sediment Nd, whereas the organic leach is impoverished in Nd (0.3–0.9%). Most Nd resides in the detrital fraction (72.2–83.3%). Overall, leached carbonate, FeMn, and organic fractions are more radiogenic than corresponding detrital fractions (Fig. 6 a). Carbonate and FeMn phases display similar Nd isotopic compositions and approach the signature of modern seawater, where seawater data is available for comparison (Canada Basin, Zimmermann et al., 2009). At further locations, the leached FeMn resemble Nd isotopic compositions of gentle FeMn leach experiments designed to extract seawater signatures from sediments (Bering and Chukchi Seas; Horikawa et al., 2010; Haley and Polyak, 2013). Except for CG3, the Nd isotope compositions of the organic fraction are generally closer to the composition of the carbonate and FeMn oxides than to the detrital pool.

Strontium incorporation into FeMn and organic fractions is minor (0.2–0.9% and 2.9–11.4%, respectively), while Sr in the carbonate fraction accounts for 14.7–60.0% of the bulk sediment Sr in the analyzed samples. $^{87}Sr/^{86}Sr$ ratios of leached carbonate and FeMn phases are similar to modern seawater (Spooner, 1976) (Fig. 6 b). We observe distinctly higher Sr isotopic ratios for the detrital phase of the samples H27, BC3, and CG3 than corresponding authigenic components and intermediate signatures for organic fractions.

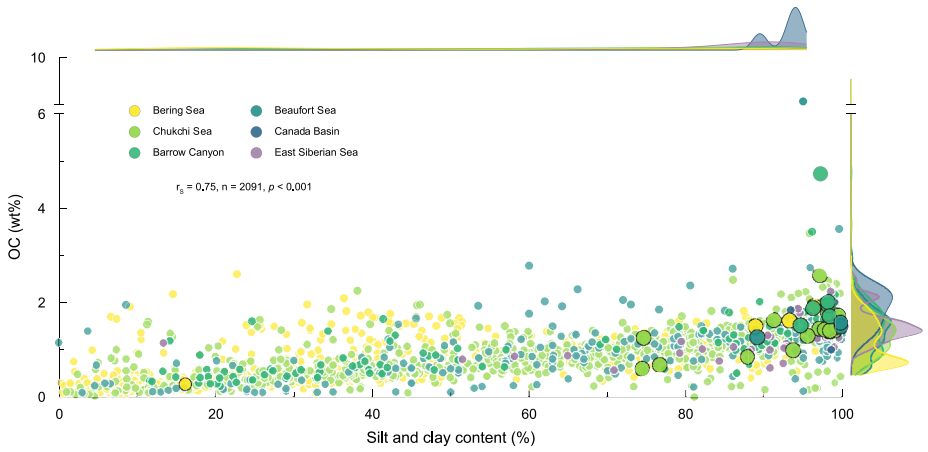

Fig. 3. Relationship between organic carbon content (OC, wt%) and summed silt and clay content (%). Density plots display relative frequencies of OC and fine-grain contents for different regions in the Western Arctic Ocean. Smaller dots correspond to literature values (see Table S4).

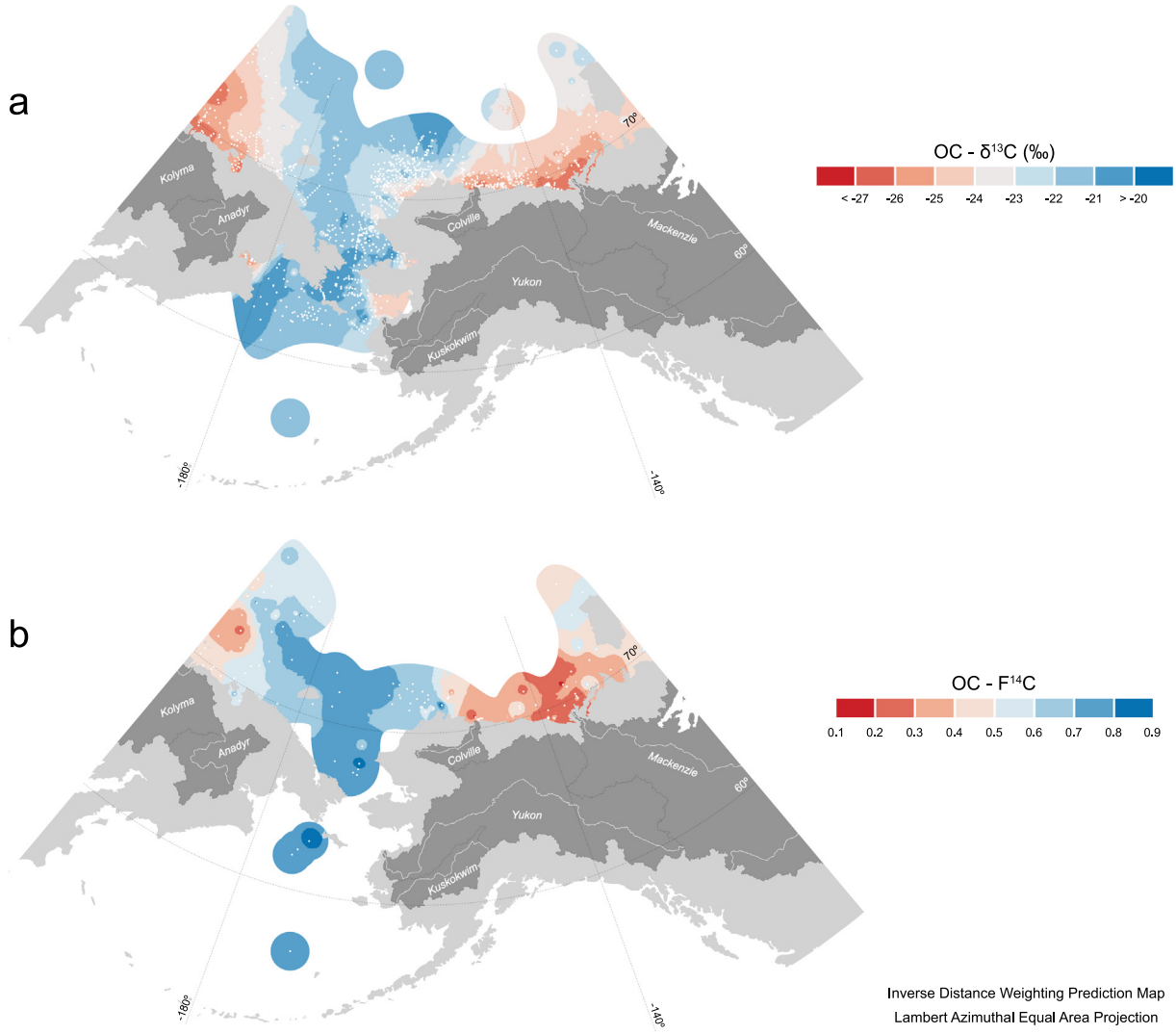

Fig. 4. Spatial distribution maps of (a) OC-$\delta^{13}C$ (‰; n = 1569) and (b) OC-$F^{14}C$ (n = 134). Maps produced using inverse distance weighting prediction. White dots represent all available observations, including literature data and data from this study. References for published values are listed in Table S4. Dark grey areas represent major river drainage basins.

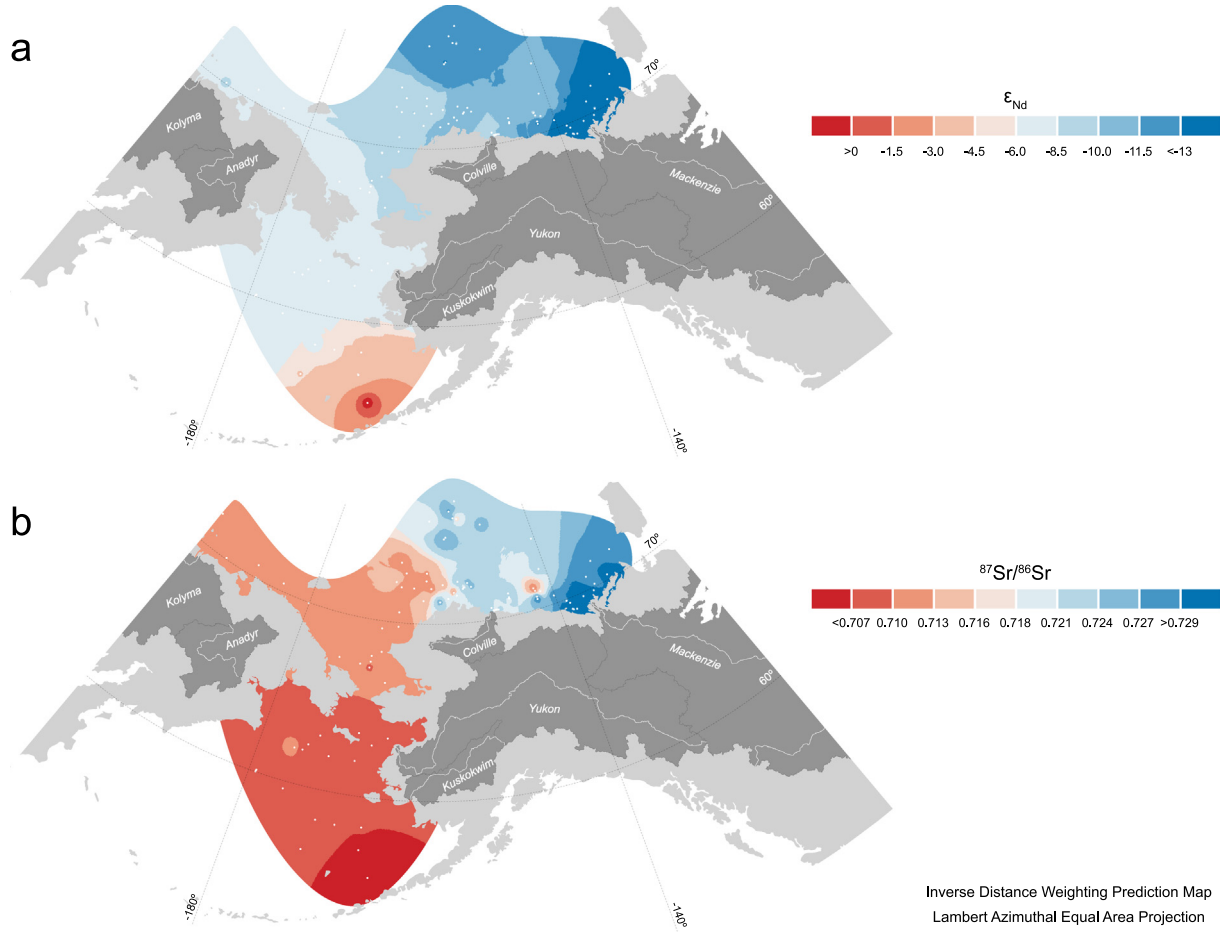

Fig. 5. Spatial distribution maps of (a) detrital ε_{Nd} (n = 94) and (b) detrital $^{87}Sr/^{86}Sr$ (n = 94). Maps produced using inverse distance weighting prediction. White dots represent all available observations, including literature data and data from this study. References for published values are listed in Table S4. Dark grey areas represent major river drainage basins.

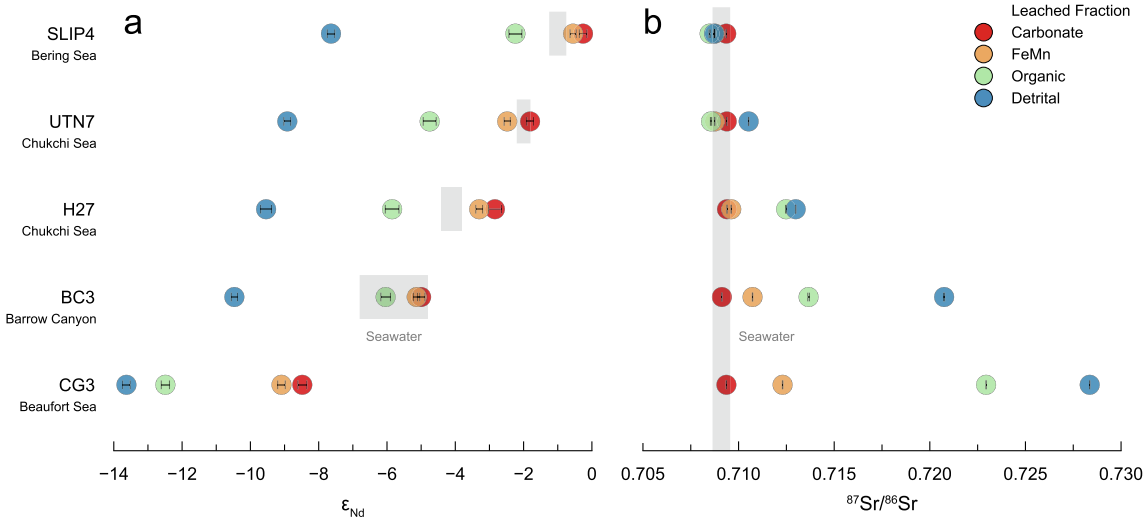

Fig. 6. (a) ε_{Nd} and (b) $^{87}Sr/^{86}Sr$ for each fraction extracted during sequential leaching. Seawater ε_{Nd} for the Barrow Canyon is from Zimmermann et al. (2009), the seawater Sr isotopic compostion from Spooner (1976). Approximate seawater ε_{Nd} for the Bering and Chukchi Seas reflect gentle FeMn leach experiments (Horikawa et al., 2010; Haley and Polyak, 2013).

5. DISCUSSION

To interpret the evolving interaction between organic matter and detrital minerals during sediment transport within this Arctic system, we first discuss the association of organic and inorganic tracers with lithogenic material and the impact of potential grain size fractionation (Section 5.1). The inorganic and organic isotopic characteristics of surface sediments are then examined in terms of the provenance of lithogenic particles (Section 5.2 and 5.3) and the transport processes influencing dispersal and spatial disposition of sediment and associated terrestrial and marine OC among the diverse sites (Section 5.4). We then merge perspectives gained by the differences in geochemical properties among sedimentary components to assess the extent to which organic and inorganic components are (de)coupled as they transit this complex, marginal sea (Section 5.5). The resultant implications are then discussed in the broader context of continental margin systems and we propose other regions that would lend themselves to the application of a coupled OC-Nd measurements to constrain trajectories of sediment dispersal (Section 5.6). Finally, we provide an outlook concerning further evolution of processes in the Western Arctic Ocean in the response to ongoing environmental and climate change.

5.1. The linkage between detrital particles, organic, and inorganic matter

In the Western Arctic Ocean, the summed silt and clay fraction of 2091 analyzed surface samples exhibits a significant positive correlation with OC content (Fig. 3) (Grebmeier et al., 2006); sediments impoverished in silt and clay generally contain less OC (OC < 0.5% for summed silt and clay < 25%). This positive relationship between the abundance of fine-grained detrital particles and OC content may reflect various processes including i) hydrodynamic sorting, ii) mineral surface area protection, and iii) the entrainment of distinct organic carbon sources which influence the preservation and distribution of organic matter in marine sediments. Lower values of OC in the coarse grain size fraction may result from winnowing of fine sediments by waves and currents, which efficiently removes fine-grained sediments and associated OC (Fig. 2) (e.g., Rearic et al., 1990; Hedges et al., 1999; Darby et al., 2009). Furthermore, coarse sediments often exhibit poor organic matter preservation potential due to diminished protection afforded by lower SA (Fig. 7 a) (e.g., Mayer, 1994a; Burdige, 2005; Blair and Aller, 2012). To assess how carbon source characteristics affect the association of lithogenic particles and OC, we compare carbon isotopic compositions of these marine surface sediments with further sediment properties (Fig. 7 b-f). Both the fraction of fine-grained sediment and Al content exhibit strong negative correlations with OC-$\delta^{13}C$ and OC-$F^{14}C$ suggesting two distinct sources of organic matter associated with lithogenic materials (Fig. 7 c-f). Pre-aged, terrestrial material in the Beaufort Sea and the Barrow Canyon sediments appears preferentially associated with fine-grained material while fresh, marine OC is found among coarser sediments with lower Al content in the Bering and Chukchi Seas. Sediments derived from volcanic arcs (e.g., Aleutian Arc) are enriched in mafic rock components and deliver aluminosilicate-poor material to adjacent oceanic margins. In contrast, the Mackenzie River exports the oldest, most-degraded POC within the fine aluminosilicate-rich fraction of the suspended load corresponding to material supplied from permafrost soils (Dellinger et al., 2014; Hilton et al., 2015).

Previous work has shown that detrital ε_{Nd} is relatively insensitive to sedimentary sorting and/or chemical weathering (Garçon et al., 2013; Bayon et al., 2015) and, as a result, ε_{Nd} serves a particularly reliable tool for continental source identification. The circumstances for ε_{Nd} as a source tracer are especially favorable for the Western Arctic given the strong isotopic contrasts in inputs, ranging between −13 for the Mackenzie River and +10 for Aleutian Arc material (see source ranges in Fig. 5 a). The positive relationship between clay content and Nd concentration (Fig. 8 a) is consistent with the mixing of clay and Nd-rich sedimentary inputs from the Mackenzie River with clay-poor, Nd-depleted inputs to the Bering Sea, including Nd-depleted arc material.

Contrasting with Nd, the relationship between the clay fraction and Sr concentrations shows two domains (Fig. 8 b). In the Bering and Chukchi Seas, clay-poor sediments show elevated Sr concentrations, which decrease with an increasing proportion of clays. In contrast, Sr concentrations in sediments from the Beaufort Sea, the Canada Basin, and on the Northwind Ridge follow a positive trend with the percentage of fine material. This non-linear relationship implies that Sr concentrations decrease with distance from both the Bering Sea and the Mackenzie River input sources, potentially explaining the lowest detrital Sr concentrations in the Chukchi Sea. Variations in Sr concentrations as a function of distance to the source could be associated with sorting effects on Sr isotope compositions (Asahara et al., 2012), however, such effects are subordinate to the isotopic variability stemming from contrasting input sources given the systematic covariation of ε_{Nd} and Sr isotope compositions across the Western Arctic (Fig. 5). Despite the clarity of patterns shown in Fig. 5 and Fig. 8, elucidation of controls on spatial variability in Sr and Nd concentrations and isotopic compositions would benefit from further delineation of source inputs, including investigation of the geochemical properties of detrital material supplied by eroding coastlines (Ping et al., 2011; Obu et al., 2017; Couture et al., 2018; Farquharson et al., 2018).

5.2. Provenance of continentally-derived lithogenic material

The main sources of lithogenic particles supplied to the Western Arctic Ocean include land drainage and coastal erosion. Such material is redistributed by currents and entrained in sea ice (Macdonald and Gobeil, 2012; Wegner et al., 2015; Macdonald et al., 2015).

The Bering Sea receives eroding volcanic rocks from the Aleutian and Kamchatka Arcs, which are the radiogenic Nd and unradiogenic Sr end-members in the studied area (Fig. 5). High ε_{Nd} values of the Aleutian Arc volcanics

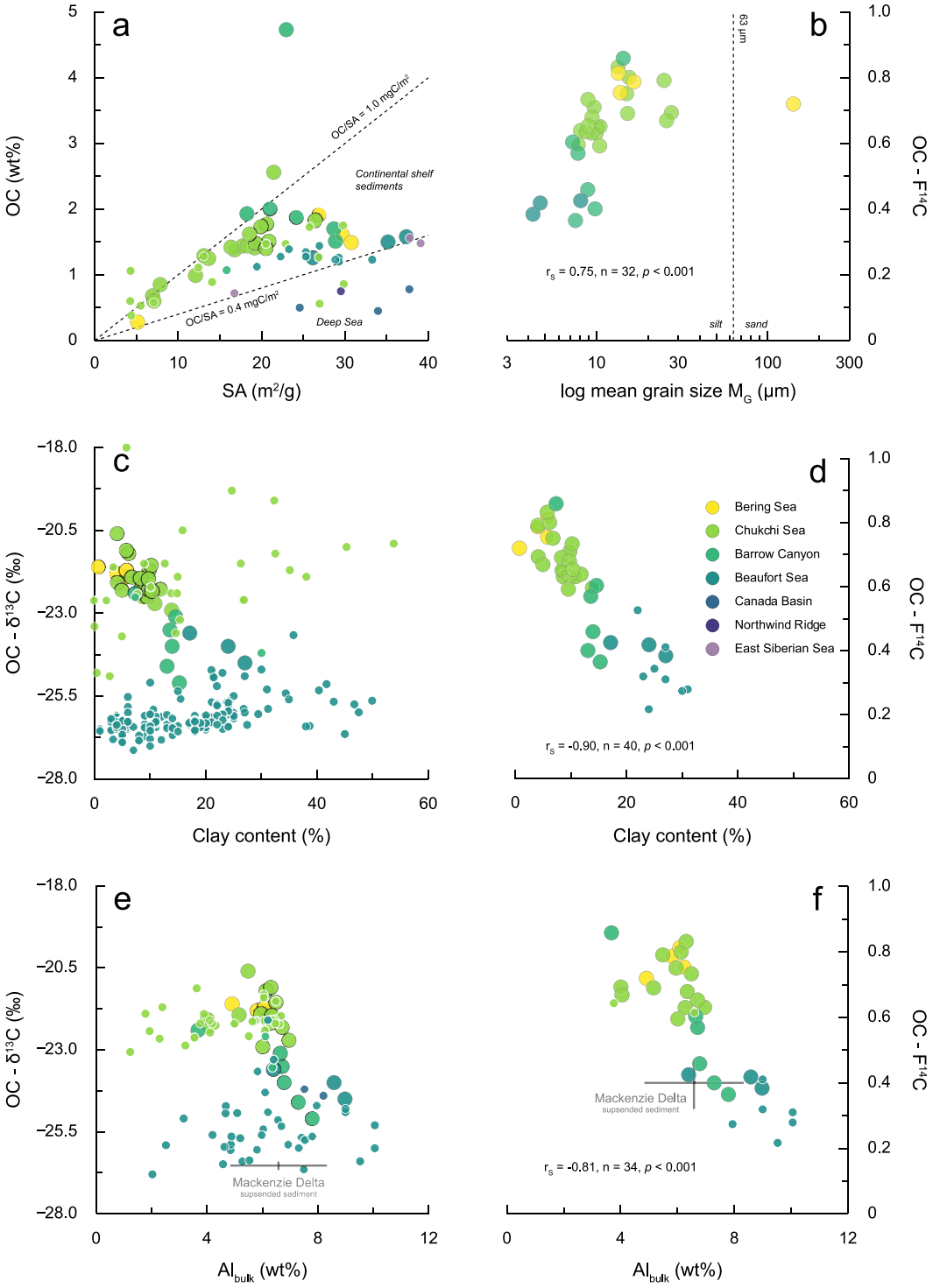

Fig. 7. Relationship between organic carbon, fine-grained contents, and Al content of marine surface sediments. (a) organic carbon content (OC, wt%) against surface area ($m^2\ g^{-1}$), (b) OC-$F^{14}C$ against log mean grain size (µm), (c) OC-$\delta^{13}C$ (‰) and (d) OC-$F^{14}C$ against clay content (%, <2 µm), (e) OC-$\delta^{13}C$ (‰) and (f) OC-$F^{14}C$ against Al content (%). Smaller dots correspond to literature values (see Table S4). The Mackenzie Delta suspended sediment end-member is given by Hilton et al. (2015).

are spatially confined to their surroundings and their contribution to the isotopic compositions observed in the northern Bering Sea is comparatively minor (SLIP1-4). Although spatial data on Sr and Nd sedimentary isotopic signatures in the Bering Sea are currently scarce, a localized influence of volcanic arc sediments on detrital Nd isotope compositions is expected due to the low sediment flux (2 Mt yr^{-1}) supplied by the Aleutian Arc (VanLaningham

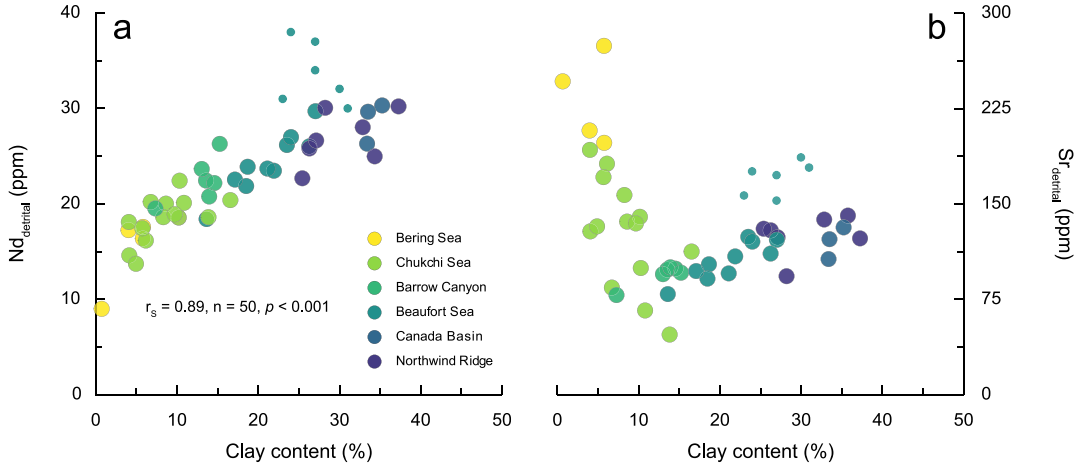

Fig. 8. Relationship between detrital (a) Nd and (b) Sr contents (ppm) and clay content (%). Smaller dots correspond to literature values (see Table S4).

et al., 2009) and low Nd concentrations for arc-derived sediments. The Aleutian source signal is mixed with less radiogenic inputs from mainly Mesozoic and Paleozoic rocks delivered to the Bering Sea by coastal erosion and fluvial input. The Yukon and Kuskokwim Rivers drain Cretaceous flysch, metamorphic and meta-sedimentary rocks ($\varepsilon_{Nd} = -8.6 \pm 0.8$, $^{87}Sr/^{86}Sr = 0.709$, Table 1) (Peucker-Ehrenbrink and Miller, 2003), while the Anadyr River drains the isotopically heterogenous Cretaceous Okhotsk-Chukotka volcanic belt ($\varepsilon_{Nd} = -0.9 \pm 5.5$, $^{87}Sr/^{86}Sr = 0.710 \pm 0.010$). The Bering Strait acts as a "melting pot" homogenizing sediments transported to the Arctic Ocean ($\varepsilon_{Nd} \sim -8.6$, $^{87}Sr/^{86}Sr \sim 0.711$) primarily influenced by the Yukon River (Asahara et al., 2012).

While the southern Chukchi Sea sediments appear to be dominated by detrital particles advected through the Bering Strait and remnants of primary production over the shelf itself, the Western portion of the Chukchi Sea receives sediments from Chukotka and the Kolyma River delivered by the Siberian Coastal Current (Chen et al., 2003; Viscosi-Shirley et al., 2003; Asahara et al., 2012). The isotopic similarity of incoming detrital material through the Bering Strait and sediment originating from northeast Siberia (Fig. 9) exacerbates source attribution based on Nd-Sr signatures. Further north in the Chukchi Sea, Nd (and Sr) isotopic signatures of surface sediments are less (more) radiogenic, which supports contributions from Mackenzie River-derived sediments transported westward along the outer Beaufort Shelf to the Chukchi Shelf via currents or sea ice (Weingartner et al., 2005), and by the Beaufort Gyre circulation further offshore (Macdonald et al., 1995; Macdonald et al., 2002; Darby, 2003; Yamamoto et al., 2017; Deschamps et al., 2018).

Detrital materials in the Beaufort Sea and the Canada Basin are characterized by less (more) radiogenic Nd (Sr) isotope compostions compared to the Chukchi Sea (Fig. 9). The major supplier of sedimentary material to the Arctic Ocean is the Mackenzie River, which drains the Proterozoic and Cambrian crust of the Canadian Shield and the Slave Province, and carries sediments with low ε_{Nd}

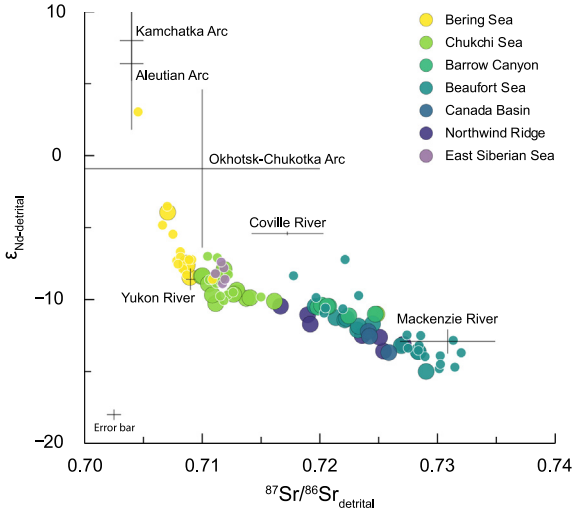

Fig. 9. Relationship between the Nd and Sr isotopic composition in the detrital phase of surface sediments, ε_{Nd} and $^{87}Sr/^{86}Sr$, in the Western Arctic Ocean. End-member compositions are listed in Table 1. Smaller dots correspond to literature values (see Table S4).

values and high Sr ratios ($\varepsilon_{Nd} = -12.91 \pm 0.84$, $^{87}Sr/^{86}Sr = 0.731 \pm 0.004$, Table 1). The influence of the Mackenzie River on Nd and Sr isotopic signatures of detrital sediments can be readily traced westward to the Colville River mouth, but, as mentioned above, likely reaches into the Chukchi Sea. The Colville contributes sediments to the Beaufort Sea with higher ε_{Nd} (−5.4) and lower Sr (0.717) values compared to the Mackenzie (Schreiner et al., 2013), potentially introducing a deviation from the mixing segment between the Mackenzie River and the sediments entering the Arctic through the Bering Strait (Fig. 9). The minor impact of the Colville River on the isotopic composition of detrital particles can be assigned to the low export of sedimentary material (5.8 Mt yr^{-1}) in comparison to the Mackenzie River (128 Mt yr^{-1}) (Arnborg et al., 1967; Carson et al., 1998). In addition to the predominating influence of Mackenzie

River sediments (Vonk et al., 2015), the Colville ε_{Nd} signal may also be further diluted by less radiogenic material stemming from coastal erosion (Jorgenson and Brown, 2005; Mars and Houseknecht, 2007; Jones et al., 2008), which also serves as a source of sediments to the region.

5.3. Sources and sinks of organic matter

Based on the dominant current systems, sources of nutrient supply, and diverging organic and inorganic compositions, the Western Arctic Ocean shelves may be categorized as inflow shelves (Bering and Chukchi Seas) and an interior shelf (Beaufort Sea) (Carmack et al., 2006; Macdonald et al., 2015). While inflow shelves commonly support high exportable primary productivity due to nutrients imported from outside the Arctic, interior shelves are characterized by subdued autochthonous input, supported mostly by shelf-edge exchange, and receive large volumes of continentally-derived material (Belicka et al., 2002; Belicka et al., 2004; Macdonald et al., 2015). The contrast between these two types of shelves is reflected at the large scale by the depletion in OC-$\delta^{13}C$ values along a south-north gradient, from the Bering to the Beaufort Sea (Fig. 10 a). The most ^{13}C-depleted signatures are observed on continental margins adjacent to Anadyr, Colville, Kuskokwim, Mackenzie, and Colville Rivers. In particular, the surface sediments in the Beaufort Sea contain a high portion of terrestrial organic matter characterized by low ^{13}C and ^{14}C isotopic values, likely introduced by the Mackenzie River (Fig. 4).

Much of the organic matter supplied to the interior Beaufort Sea by the Mackenzie and, to a lesser degree, by the Colville River has experienced extensive pre-aging in terrestrial reservoirs, including permafrost soils, lacustrine, and deltaic environments, prior to export and accumulation in marine sediments (Belicka et al., 2002; Belicka et al., 2004; Drenzek et al., 2007; Belicka and Harvey, 2009; Hilton et al., 2015; Feng et al., 2015; Zhang et al., 2017; Vonk et al., 2019). Contributions from modern terrestrial primary production, characterized by high OC-$F^{14}C$ values, are thus minor for POC exported by the Mackenzie River and Colville River (Fig. 10 b; e.g., Vonk et al., 2019), consistent with efficient degradation of this OC pool (Yunker and Macdonald, 1995; Goñi et al., 2005; Yunker et al., 2011).

The $\delta^{13}C$ signatures of marine biomass (−20 to −26‰) in the Western Arctic Ocean can approach those of terrigenous inputs, limiting the use of stable carbon isotopes in source apportionment. Slow-growing marine phytoplankton preferentially incorporates isotopically light (^{13}C-depleted) carbon under high pCO_2, low temperature and light conditions (Goericke and Fry, 1994; Schubert and Calvert, 2001; Henley et al., 2012; Zhang et al., 2012; Pineault et al., 2013). Furthermore, DIC in the Canada Basin, which sustains phytoplankton growth, is more ^{13}C-depleted than surrounding ocean regions (Griffith et al., 2012). Similarly, ice algae can locally contribute significantly to the phytoplankton biomass and show highly variable ^{13}C values in the Chukchi and Beaufort Seas (Belicka et al., 2004; Belicka and Harvey, 2009; Gradinger, 2009). Nevertheless, old ages of OC (low $F^{14}C$ values; Fig. 4 b) in the analyzed surface sediments indicate that marine OC is efficiently recycled within the water column or by the benthos, while terrestrial OC is preferentially buried on the interior shelves and subject to off-shelf export (Macdonald et al., 1998; De Haas et al., 2002; Goñi et al., 2005).

Coastal erosion releases significant amounts of OC to nearshore waters of the northern Chukchi and western Beaufort Seas along the Alaskan shoreline (Jorgenson and Brown, 2005; Mars and Houseknecht, 2007; Jones et al., 2008; Ping et al., 2011; Lantuit et al., 2012). Although eroded coastal material is mostly trapped nearshore, carbon isotopic signatures indicate that mobilization and cross-shelf transfer occurs along the northwestern Alaskan shore (Fig. 4), likely induced by wave action associated with the

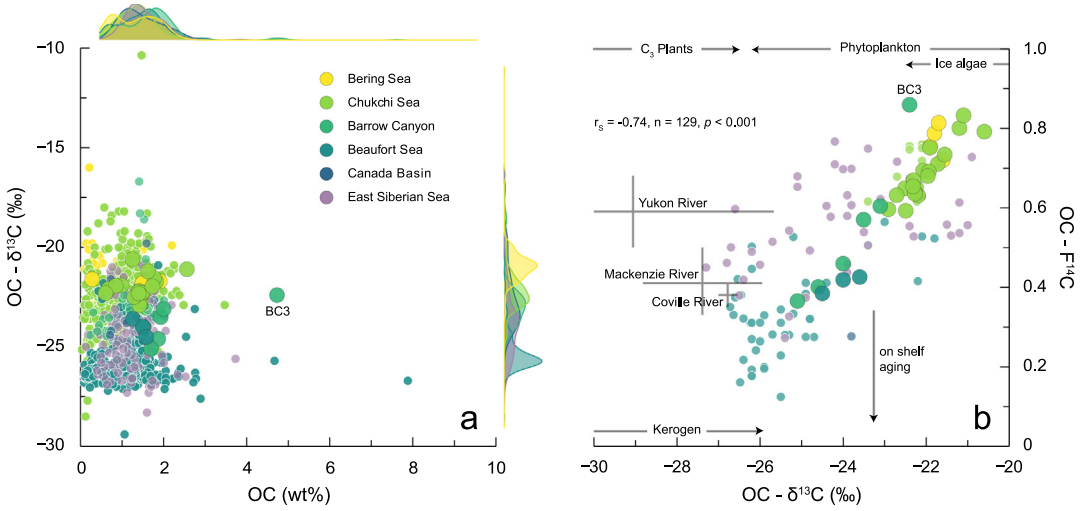

Fig. 10. Relationships between OC-$\delta^{13}C$ (‰) and (a) organic carbon content (OC, wt%) and (b) OC-$F^{14}C$. Density curves display relative frequencies of OC-$\delta^{13}C$ and the OC contents for regions in the Western Arctic Ocean. End-member compositions are listed in Table 1. Smaller dots correspond to literature values (see Table S4).

lengthening of the open water season and the increasing frequency of storms (Yu et al., 2014).

In contrast, open shelf regions of the Bering and Chukchi Seas receive larger contributions of fresh marine organic matter, evident in the enriched ^{13}C and ^{14}C signatures of OC in surface sediments (Fig. 10 b). Cold and nutrient-rich Pacific water transported within the Anadyr and Bering Shelf Currents supports exportable marine productivity close to the northeastern Siberian coast (Springer and McRoy, 1993; Grebmeier et al., 2006). Pacific water inflow passes through the Bering Strait, across the Chukchi Shelf and is then funneled through the Middle Channel, the Herald, and Barrow Canyon (Weingartner et al., 2005; Pickart et al., 2016), sustaining planktonic and benthic food webs (Walsh et al., 2004; Woodgate and Aagaard, 2005; Grebmeier et al., 2006; Christensen et al., 2008).

Submarine canyons incising the Chukchi and Beaufort Shelves are important geomorphic features in the Western Arctic Ocean (Harris and Whiteway, 2011). Canyons act as "hot spots" for primary productivity driven by wind-forced upwelling in or near canyon heads. In addition, submarine canyons are conduits for shelf-basin exchange and passively funnel terrestrial material offshore (Harris and Whiteway, 2011; Puig et al., 2014). The ^{13}C-, and ^{14}C-enriched signatures of surface sediments recovered from the upper Barrow Canyon (BC3: OC-$\delta^{13}C = -22.4$, OC-$F^{14}C = 0.86$) suggest recent carbon supply from persistent phytoplankton blooms, consistent with in-situ samples and remote sensing studies (Lalande et al., 2007; Lepore et al., 2007; Christensen et al., 2008; Lowry et al., 2015; Pisareva et al., 2019). In contrast, sediments in the lower Barrow Canyon exhibit depleted OC isotopic compositions (Fig. 10) indicating preferential transfer and burial of terrigenous material from coastal regions (Goñi et al., 2013). The abundance of vascular plant-derived biomarkers in Barrow Canyon sediments further illustrates the significance of canyon facilitated transport of terrestrial matter (Belicka and Harvey, 2009; Goñi et al., 2013). Similar distributions of carbon signatures are expected for the Mackenzie Trough and the Kugmallit Canyon, which are directly supplied by sedimentary material from the Mackenzie River (Carmack and Kulikov, 1998; Williams et al., 2008; Osborne and Forest, 2016) and show isotopic gradients in sediments (McMahon et al., 2021). Analogous to the Barrow Canyon, primary productivity is supported by upwelling in or near the canyon heads, while cross shelf-export of riverine particulates occurs at depth (Macdonald et al., 1987; O'Brien et al., 2006; Forest et al., 2007). The inorganic isotopic composition of the Barrow Canyon sediments is relatively uniform ($\varepsilon_{Nd} = -10.7 \pm 0.3$, $^{87}Sr/^{86}Sr = 0.721 \pm 0.002$, n = 4, Table S3) and resembles signatures observed in sediments from the Colville River Delta indicating an effective funneling of adjacent coastal material (Table 1).

Similar to the binary mixing trend of OC isotopes with Al (Section 5.1, Fig. 7 f), a simple linear relationship between OC-$\delta^{13}C$ and OC-$F^{14}C$ captures most of the OC isotopic variability in surface sediments of the Western Arctic Ocean (Fig. 10 b). The marine OC end-member is defined by high OC-$\delta^{13}C$ and OC-$F^{14}C$ values reflecting modern surface ocean biological productivity (see Section 3.6.3.; Table 1) (Fischer, 1991; Hobson et al., 1995; Schubert and Calvert, 2001; Stein and Macdonald, 2004). The terrigenous OC end-member, on the other hand, represents the isotopic composition of fluvial suspended POC of the Mackenzie River, including soils and peat, as well as fossil OC originating from eroding bedrock strata. The OC isotopic composition of surface sediments from the Mackenzie and Colville shelf sediments falls below the riverine OC-$F^{14}C$ compositions and approaching the compositional range of kerogen. We attribute the deviation from the binary mixing to the aging of both marine and terrestrial OC during repeated cycles of resuspension and deposition during across-, and along-shelf transport (Bao et al., 2018a, 2018b, 2018c; Bröder et al., 2018).

5.4. Hydrographic influence on sediment dispersal in the Western Arctic Ocean

Several hydrodynamic processes are involved in short-, and long-range dispersion of organic and inorganic particles supplied to the Western Arctic Ocean. On continental margins, sedimentary material is subject to repeated resuspension-deposition cycles induced by wind and tidal forcing and storm wave action (Lintern et al., 2013). Cross-shelf and off-shore advection of detrital particles is also promoted by ice-rafting of sediment initiated by processes like suspension freezing, bottom grounding, and overflooding (Rearic et al., 1990; Reimnitz et al., 1998; Tütken et al., 2002; Darby et al., 2009), turbidite flows (Grantz et al., 1999), shelfbreak eddies (D'Asaro, 1988; Pickart, 2004; Mathis et al., 2007; Spall et al., 2008; O'Brien et al., 2013; Watanabe et al., 2014), and via funneling down submarine canyons (Macdonald et al., 1987; Williams et al., 2008). This lateral transfer is observed in intermediate nepheloid layers laden with lithogenic sediment and captured by sediment traps located in canyons and on outer shelf regions (O'Brien et al., 2006; Forest et al., 2007; Gardner et al., 2018; Deschamps et al., 2018). The majority of sinking particulate matter in the central Canada Basin consists of detrital material, highlighting the role of horizontal across-margin sediment transfer (Hwang et al., 2008; Hwang et al., 2015).

Localized lateral displacement processes occurring along the northern Alaskan and Canadian coast are regionally important, but at a large scale, sediment transport patterns are dictated by major surface and subsurface currents. The anticyclonic Beaufort Gyre provides a large-scale westward surface flow on the outer Beaufort Shelf. Sediments resuspended over the outer shelf and slope and sediment associated with sea ice drifting within the Beaufort Gyre are transported westward along the margin. This pattern of sediment dispersal is consistent with the observed spatial distribution of detrital Nd and Sr isotopic signatures (Fig. 5). Notably, Nd and Sr isotopic values of surface sediments collected from the Northwind Ridge are similar to those of the Mackenzie River, underlining the importance of the Beaufort Gyre as a conduit for shelf-basin sediment transfer. Coastal currents such as the Anadyr, the Alaskan Coastal Current, and shelfbreak jets along the North

American coast vary strongly seasonally in their strength and direction obscuring transport patterns (Macdonald et al., 2002; Yamamoto-Kawai et al., 2009; Schulze and Pickart, 2012).

5.5. Neodymium and its isotope compositions in organic matter

The marked spatial gradients in carbon (^{13}C and ^{14}C) and Nd isotopic compositions of surface sediments in the Western Arctic Ocean provide a means to constrain the provenance of both organic matter and detrital sediments, and to explore the evolution of organo-mineral associations in a source to sink context.

As described above (Section 5.3), carbon isotopes yield direct information of the origin, age, and fate of OC accumulating in surface sediments. Conceptually, Nd isotopes may yield similar information provided Nd associated with organic matter can be reliably extracted from marine sediments and the marine and terrestrial source Nd isotope signatures can be constrained. Previous work suggested that rare earth elements (REE, including Nd) associated with organic matter can be leached reliably based on distinct and reproducible REE patterns (Freslon et al., 2014). These authors also found close agreement between Nd isotope compositions in terrestrial sediments and associated organic matter, consistent with a congruent release of Nd isotopes to the hydrosphere during weathering (e.g., Bayon et al., 2006; Rickli et al., 2013) and subsequent incorporation (of a likely minute fraction) into organic matter. The detrital fraction in sediments, hence, may serve as a proxy for the Nd isotope composition of terrestrial organic matter. Similarly, leached FeMn phases are a suitable proxy for the Nd isotope composition of seawater (e.g., Gutjahr et al., 2007), incorporated in marine OC.

Assuming similar Nd concentrations in marine and terrestrial OC, the leached ε_{Nd} signatures in organic matter can be converted to terrestrial and marine OC fractions. There is reasonable agreement between the terrigenous OC fraction computed from Nd isotopes and the one calculated by the Bayesian dual carbon isotope (OC-$\delta^{13}C$, OC-$F^{14}C$) model, albeit for a limited sample suite (Fig. 11 a). Further measurements are clearly required to rigorously test and validate these findings, including the use of improved protocols to selectively extract Nd seawater signals from marine sediments (e.g., Gutjahr et al., 2007; Blaser et al., 2016) and refinement of organic matter leaching procedures (see below).

Although it may seem surprising to find measurable amounts of REE associated with organic material, one should note that REE concentrations appear to be quite variable from 1.5 to 50 μg per g of organic matter (Freslon et al., 2014) but not high enough to be significant for the bulk sediment REE budgets (<1% in the samples studied here, see Section 4.3.2). A range of processes are known in terrestrial and marine environments that document association of organic matter and REE, which, taken together, illustrate that REE are expected to be found in organic matter. REE are complexed by humic acids in rivers (Sonke and Salters, 2006; Pourret et al., 2007), they are scavenged onto organic colloids (Stolpe et al., 2013) and they reside in the organic fraction of sediments (Freslon et al., 2014). REE in ambient seawater can be adsorbed onto the surface of organics or assimilated by organisms (Takahashi et al., 2005; Christenson and Schijf, 2011; Haley et al., 2014).

For future applications, it will be important to further investigate the controls on REE concentrations in organic matter. Such an understanding is relevant to assess Nd contributions from marine and terrestrial organic matter to the bulk organic fraction in sediments. Furthermore, leaching methods for organic fractions may introduce some bias; the approach used here and in Freslon et al. (2014) following Tessier et al. (1979) is presumably more effective for fresh and reactive OC, while old, refractory organic matter, for instance emanating from permafrost soils, will be leached less efficiently. Nevertheless, our preliminary results confirm that Nd isotopes in OC can provide constraints on the origin of organic matter (Freslon et al., 2014) complementing the use of detrital Nd isotopes for the distinction of continental source areas.

5.6. Implications and broader relevance

Due to the intrinsic variability in carbon and Nd/Sr isotopic signatures, the Western Arctic Ocean and its surroundings serve as a natural laboratory to assess the extent to which terrestrially-derived particulate organic matter retains an association with its detrital mineral host during delivery, dispersal, and burial, and how it intermingles with marine biogenic materials on continental margins. Although more detrital ε_{Nd} data are needed to fully delineate transport pathways over Western Arctic continental shelves and into the deep basin, combining detrital Nd and organic carbon isotopic signatures allows for regional erosional sources of detrital sedimentary particles and associated OC to be traced in the marine environment, and reveals sustained coupling between organic matter and its mineral host. Although the pronounced isotopic gradients in the Western Arctic Ocean lends themselves to this dual source tracking approach, strong isotopic contrasts in other regions of the Arctic (Guo et al., 2004; Porcelli et al., 2009), as well as in other continental margin systems, including the South Chinese Sea (Yang et al., 2007; Dou et al., 2012; Van der Voort et al., 2018; Bao et al., 2019; Xu et al., 2019) and the northwest Atlantic margin (Hwang et al., 2021), may allow for the adoption of similar approaches to delineate trajectories of lithogenic particles and associated OC transport in the ocean.

Arctic climate change manifested as increasing surface temperatures and large-scale alteration of the cryosphere (sea ice diminution, permafrost thaw), will affect Arctic terrestrial and marine carbon cycles (Graversen et al., 2008; Cohen et al., 2014). These effects have the potential to impact the climate system through manifold positive feedback mechanisms (McGuire et al., 2006). The ongoing loss of multi-year sea ice in the Arctic Ocean may promote marine primary production and increased fluxes of biogenic material to the seafloor over the Arctic shelves and slopes (Grebmeier et al., 2010; McGuire et al., 2010; Morison

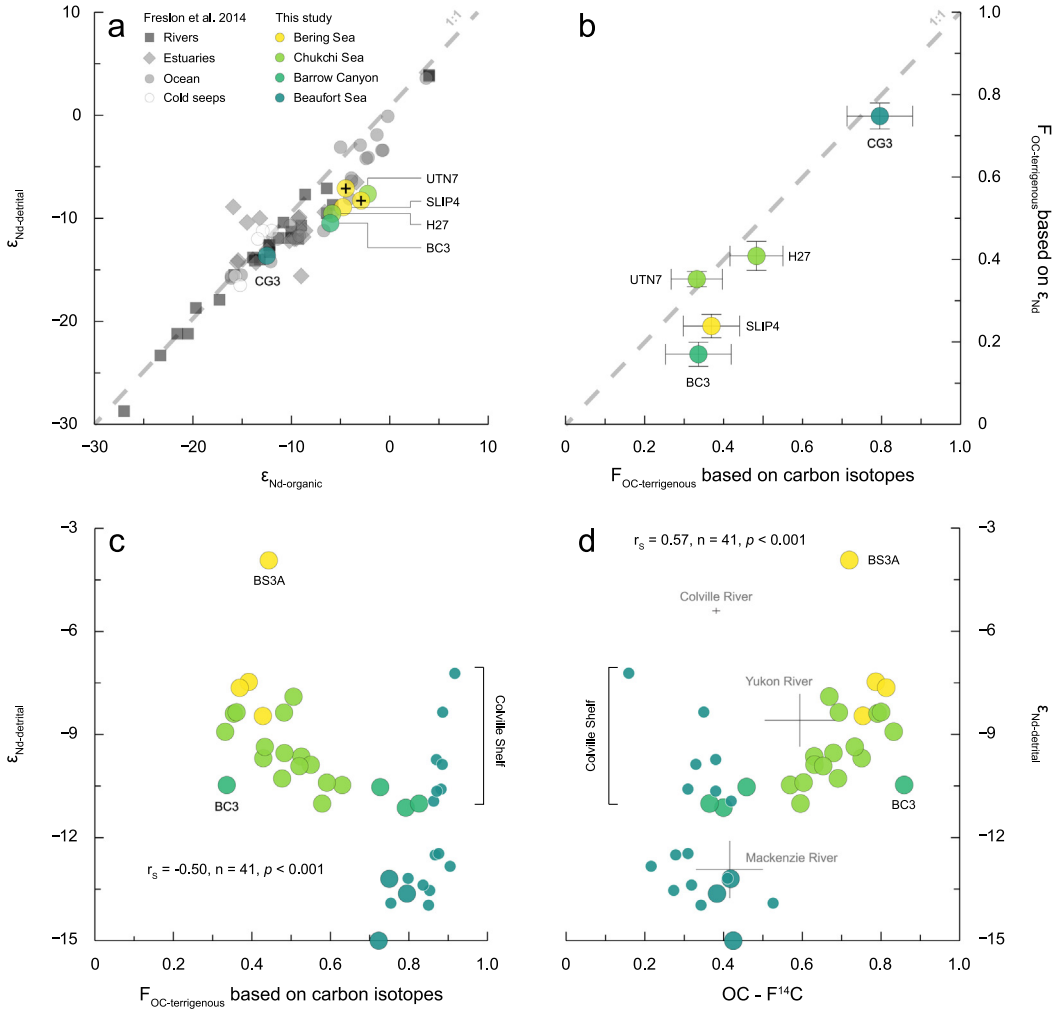

Fig. 11. (a) Relationship between ε_{Nd} of detrital sediments and organic leachates observed in the different settings. Markers augmented by crosses refer to Asahara et al. (2012). (b) Correlation between the estimated terrigenous fraction of OC using Nd isotopes and carbon isotopic compositions (see Section 3.6.3 and 5.5. for more details). Dashed line shows 1:1 correspondence. ε_{Nd} of the detrital phase as a function of (c) the terrigenous fraction derived from carbon isotopes and (d) OC-$F^{14}C$. End-member compositions are listed in Table 1. Small dots correspond to literature values (see Table S4).

et al., 2012; Arrigo and van Dijken, 2015; Notz and Stroeve, 2016). Concomitantly, fluxes of terrigenous POC and associated materials to the Arctic Ocean will be enhanced by the thawing of permafrost in drainage basins and soils in coastal regions (Lantuit et al., 2012; Fritz et al., 2017; Rood et al., 2017). The increased input of terrestrial organic and lithogenic material and likely positive response by marine primary production to nutrient inflows associated with these changes will significantly impact and modify geochemical cycles and benthic-pelagic coupling via the transfer, deposition, and burial of carbon in this marginal sea. In parallel, the Western Arctic Ocean and its marine ecosystems are experiencing dramatic change, which is likely to increase into the future. The sources, transport pathways, and depositional centers of organic and inorganic particles examined in the present investigation provide vital context and a baseline against which to identify future regional change.

6. SUMMARY AND CONCLUSIONS

To our knowledge, this study represents the first attempt to combine the relationships between detrital Nd (and Sr) isotopic signatures and carbon isotope characteristics of OC in marine sediments to assess terrigenous organic matter-mineral associations in a source to sink context. Strong spatial contrasts in carbon (^{13}C and ^{14}C) and Nd (and Sr) isotopic compositions of input sources provide a window on the provenance and transport pathways of detrital sediments and associated organic matter in the Western Arctic Ocean.

Terrigenous sediments introduced by fluvial export and coastal erosion along the North American continental margin host old, terrestrial carbon that is remobilized and laterally transported across the shelf, likely by ice rafting, in plumes and eddies, and funneling through canyons. Nd and Sr isotopic compositions suggest that the

Beaufort Gyre promotes the dispersal of lithogenic material farther offshore, to the west, and into the interior Canada Basin. In contrast, the Bering and Chukchi Seas receive nutrient-rich waters of Pacific origin, which favor high marine primary productivity and the export of autochthonous organic matter from surface waters to underlying sediments, as evidenced by their ^{13}C-, and ^{14}C-enriched carbon isotopic compositions. Detrital sediments in the Bering and Chukchi Seas reflect the input of eroding radiogenic volcanic arc material as well as less radiogenic lithogenic particles emanating from the Anadyr, Kuskokwim, and Yukon Rivers.

The relationship between sedimentological properties, Al content, and OC-^{14}C indicates a strong association of terrigenous OC with lithogenic particles. In particular, sediment provenance and transport pathways delineated from coupled carbon and Nd isotopic data suggest a close "partnership" between detrital particles and organic matter during export, dispersal, and accumulation. We present evidence that both organic (e.g., OC-^{14}C) and inorganic (e.g., ε_{Nd}) isotopes may serve as strong indicators of the source of detrital particles and associated OC in the water column and underlying sediments. The estimation of marine and terrestrial OC contributions based on leached organic ε_{Nd} signatures mirrors the apportionments derived from carbon isotopic compositions further stressing the coupling of carbon and Nd.

The combined OC-^{14}C and Nd isotopic measurement approach applied in this study holds promise for furthering our understanding of the coupling of organic and inorganic terrigenous materials during source-to-sink transport, and for constraining regional OC budgets and carbon burial. Further studies are necessary to elucidate underlying processes, assess diagenetic transformations, and understand the influence of ongoing regional ocean and climate change on OC sequestration.

Declaration of Competing Interest

The authors declare that they have no known competing financial interests or personal relationships that could have appeared to influence the work reported in this paper.

ACKNOWLEDGMENTS

This work was supported by the Swiss National Science Foundation through the grant SNF200020_163162/1, "CAPS-LOCK II" and SNF200020_184865/1, "CAPS-LOCK III". We thank Al Gagnon, Ellen Roosen, and Glen Jones for providing core-top samples from the core repository at the Woods Hole Oceanographic Institution (WHOI), and Daniel Montluçon and Michael Strupler for assistance with mineral surface area and grain size measurements. We also acknowledge comprehensive and valuable comments of two anonymous reviewers. All data generated for this study is provided in the supplementary information. The authors declare no conflict of interest. All of the authors have approved the contents of this paper and have agreed to Elsevier submission policies.

APPENDIX A. SUPPLEMENTARY MATERIAL

Supplementary data to this article can be found online at https://doi.org/10.1016/j.gca.2021.08.019.

REFERENCES

Aagaard K. and Carmack E. C. (1989) The role of sea ice and other fresh water in the Arctic circulation. *J. Geophys. Res.* **94**, 14485–14498.

Arnborg L., Walker H. J. and Peippo J. (1967) Suspended load in the Colville River, Alaska, 1962. *Geogr. Ann.* **49A**, 131–144.

Arrigo K. R. and van Dijken G. L. (2015) Continued increases in Arctic Ocean primary production. *Prog. Oceanogr.* **136**, 60–70.

Asahara Y., Takeuchi F., Nagashima K., Harada N., Yamamoto K., Oguri K. and Tadai O. (2012) Provenance of terrigenous detritus of the surface sediments in the Bering and Chukchi Seas as derived from Sr and Nd isotopes: Implications for recent climate change in the Arctic regions. *Deep Res. Part II Top. Stud. Oceanogr.* **61–64**, 155–171.

Backman J., Jakobsson M., Løvlie R., Polyak L. and Febo L. A. (2004) Is the central Arctic Ocean a sediment starved basin? *Quat. Sci. Rev.* **23**, 1435–1454.

Bao R., Blattmann T. M., McIntyre C., Zhao M. and Eglinton T. I. (2019) Relationships between grain size and organic carbon ^{14}C heterogeneity in continental margin sediments. *Earth Planet. Sci. Lett.* **505**, 76–85.

Bao R., McIntyre C., Zhao M., Zhu C., Kao S. J. and Eglinton T. I. (2016) Widespread dispersal and aging of organic carbon in shallow marginal seas. *Geology* **44**, 791–794.

Bao R., McNichol A. P., McIntyre C. P., Xu L. and Eglinton T. I. (2018a) Dimensions of radiocarbon variability within sedimentary organic matter. *Radiocarbon* **60**, 775–790.

Bao R., Uchida M., Zhao M., Haghipour N., Montluçon D., McNichol A., Wacker L., Hayes J. M. and Eglinton T. I. (2018b) Organic carbon aging during across-shelf transport. *Geophys. Res. Lett.* **45**, 8425–8434.

Bao R., van der Voort T. S., Zhao M., Guo X., Montluçon D. B., McIntyre C. and Eglinton T. I. (2018c) Influence of hydrodynamic processes on the fate of sedimentary organic matter on continental margins. *Global Biogeochem. Cycles* **32**, 1420–1432.

Bayon G., German C. R., Boella R. M., Milton J. A., Taylor R. N. and Nesbitt R. W. (2002) An improved method for extracting marine sediment fractions and its application to Sr and Nd isotopic analysis. *Chem. Geol.* **187**, 179–199.

Bayon G., Toucanne S., Skonieczny C., Andre L., Bermell S., Cheron S., Dennielou B., Etoubleau J., Freslon N., Gauchery T., Germain Y., Jorry S. J., Menot G., Monin L., Ponzevera E., Rouget M. L., Tachikawa K. and Barrat J. A. (2015) Rare earth elements and neodymium isotopes in world river sediments revisited. *Geochim. Cosmochim. Acta* **170**, 17–38.

Bayon G., Vigier N., Burton K. W., Brenot A., Carignan J., Etoubleau J. and Chu N. C. (2006) The control of weathering processes on riverine and seawater hafnium isotope ratios. *Geology* **34**, 433–436.

Belicka L. L. and Harvey H. R. (2009) The sequestration of terrestrial organic carbon in Arctic Ocean sediments: A comparison of methods and implications for regional carbon budgets. *Geochim. Cosmochim. Acta* **73**, 6231–6248.

Belicka L. L., Macdonald R. W., Yunker M. B. and Harvey H. R. (2004) The role of depositional regime on carbon transport and preservation in Arctic Ocean sediments. *Mar. Chem.* **86**, 65–88.

Belicka L., Macdonald R. and Harvey H. (2002) Sources and transport of organic carbon to shelf, slope, and basin surface

sediments of the Arctic Ocean. *Deep Sea Res. Part I Oceanogr. Res. Pap.* **49**, 1463–1483.
Bennett R. H., Hulbert M. H., Curry K. J., Curry A. and Douglas J. (2012) Organic matter sequestered in potential energy fields predicted by 3-D clay microstructure model. Direct observations of organo-clay micro- and nanofabric. *Mar. Geol.* **315–318**, 108–114.
Bianchi T. S., Cui X., Blair N. E., Burdige D. J., Eglinton T. I. and Galy V. (2018) Centers of organic carbon burial and oxidation at the land-ocean interface. *Org. Geochem.* **115**, 138–155.
Blair N. E. and Aller R. C. (2012) The fate of terrestrial organic carbon in the marine environment. *Ann. Rev. Mar. Sci.* **4**, 401–423.
Blaser P., Lippold J., Gutjahr M., Frank N., Link J. M. and Frank M. (2016) Extracting foraminiferal seawater Nd isotope signatures from bulk deep sea sediment by chemical leaching. *Chem. Geol.* **439**, 189–204.
Blott S. J. and Pye K. (2001) Gradistat: A grain size distribution and statistics package for the analysis of unconsolidated sediments. *Earth Surf. Process. Landforms* **26**, 1237–1248.
Bock M. J. and Mayer L. M. (2000) Mesodensity organo-clay associations in a near-shore sediment. *Mar. Geol.* **163**, 65–75.
Bröder L., Tesi T., Andersson A., Semiletov I. and Gustafsson Ö. (2018) Bounding cross-shelf transport time and degradation in Siberian-Arctic land-ocean carbon transfer. *Nat. Commun.* **9**, 1–8.
Burdige D. J. (2005) Burial of terrestrial organic matter in marine sediments: A re-assessment. *Global Biogeochem. Cycles* **19**, 1–7.
Burdige D. J. (2007) Preservation of organic matter in marine sediments: Controls, mechanisms, and an imbalance in sediment organic carbon budgets? *Chem. Rev.* **107**, 467–485.
Campeau A., Soerensen A. L., Martma T., Åkerblom S. and Zdanowicz C. (2020) Controls on the ^{14}C content of dissolved and particulate organic carbon mobilized across the Mackenzie River Basin, Canada. *Global Biogeochem. Cycles* **34**, 1–15.
Canuel E. A., Cammer S. S., McIntosh H. A. and Pondell C. R. (2012) Climate change impacts on the organic carbon cycle at the land-ocean interface. *Annu. Rev. Earth Planet. Sci.* **40**, 685–711.
Carmack E., Barber D., Christensen J., Macdonald R., Rudels B. and Sakshaug E. (2006) Climate variability and physical forcing of the food webs and the carbon budget on panarctic shelves. *Prog. Oceanogr.* **71**, 145–181.
Carmack E. C. and Kulikov E. A. (1998) Wind-forced upwelling and internal Kelvin wave generation in Mackenzie Canyon, Beaufort Sea. *J. Geophys. Res. Ocean.* **103**, 18447–18458.
Carson M. A., Conly F. M. and Jasper J. N. (1999) Riverine sediment balance of the Mackenzie Delta, northwest territories, Canada. *Hydrol. Process.* **13**, 2499–2518.
Carson M. A., Jasper J. N. and Conly F. M. (1998) Magnitude and sources of sediment input to the Mackenzie Delta, Northwest Territories. *Arctic* **51**, 116–124.
Chen Z., Gao A., Liu Y., Sun H., Shi X. and Yang Z. (2003) REE geochemistry of surface sediments in the Chukchi Sea. *Sci. China Ser. D Earth Sci.* **46**, 603–611.
Christensen J. P., Shimada K., Semiletov I. and Wheeler P. A. (2008) Chlorophyll Response to Shelf-Break Upwelling and Winds in the Chukchi Sea, Alaska, in Autumn. *Open Oceanogr. J.* **2**, 34–53.
Christenson E. A. and Schijf J. (2011) Stability of YREE complexes with the trihydroxamate siderophore desferrioxamine B at seawater ionic strength. *Geochim. Cosmochim. Acta* **75**, 7047–7062.
Coachman L. K., Aagaard K. and Tripp R. D. (1975) *Bering Strait, The Regional Physical Oceanography*. University of Washington Press, Seatlle and London.
Cohen J., Screen J. A., Furtado J. C., Barlow M., Whittleston D., Coumou D., Francis J., Dethloff K., Entekhabi D., Overland J. and Jones J. (2014) Recent Arctic amplification and extreme mid-latitude weather. *Nat. Geosci.* **7**, 627–637.
Cooper L. W., Lalande C., Pirtle-Levy R., Larsen I. L. and Grebmeier J. M. (2009) Seasonal and decadal shifts in particulate organic matter processing and sedimentation in the Bering Strait Shelf region. *Deep Res. Part II Top. Stud. Oceanogr.* **56**, 1316–1325.
Corlett W. B. and Pickart R. S. (2017) The Chukchi slope current. *Prog. Oceanogr.* **153**, 50–65.
Couture N. J., Irrgang A., Pollard W., Lantuit H. and Fritz M. (2018) Coastal erosion of permafrost soils along the Yukon coastal plain and fluxes of organic carbon to the Canadian Beaufort Sea. *J. Geophys. Res. Biogeosci.* **123**, 406–422.
Curry K. J., Bennett R. H., Mayer L. M., Curry A., Abril M., Biesiot P. M. and Hulbert M. H. (2007) Direct visualization of clay microfabric signatures driving organic matter preservation in fine-grained sediment. *Geochim. Cosmochim. Acta* **71**, 1709–1720.
D'Asaro E. A. (1988) Observations of Small Eddies in the Beaufort Sea. *J. Geophys. Res.* **93**, 6669–6684.
Danielson S. L., Eisner L., Ladd C., Mordy C., Sousa L. and Weingartner T. J. (2017) A comparison between late summer 2012 and 2013 water masses, macronutrients, and phytoplankton standing crops in the northern Bering and Chukchi Seas. *Deep Res. Part II Top. Stud. Oceanogr.* **135**, 7–26.
Darby D. A. (2003) Sources of sediment found in sea ice from the western Arctic Ocean, new insights into processes of entrainment and drift patterns. *J. Geophys. Res. C Ocean.* **108**, 1–10.
Darby D. A., Ortiz J., Polyak L., Lund S., Jakobsson M. and Woodgate R. A. (2009) The role of currents and sea ice in both slowly deposited central Arctic and rapidly deposited Chukchi-Alaskan margin sediments. *Glob. Planet. Change* **68**, 58–72.
Dellinger M., Gaillardet J. Ô., Bouchez J., Calmels D., Galy V., Hilton R. G., Louvat P. and France-Lanord C. (2014) Lithium isotopes in large rivers reveal the cannibalistic nature of modern continental weathering and erosion. *Earth Planet. Sci. Lett.* **401**, 359–372.
Deniel C. and Pin C. (2001) Single-stage method for the simultaneous isolation of lead and strontium from silicate samples for isotopic measurements. *Anal. Chim. Acta* **426**, 95–103.
Deschamps C. E., Montero-Serrano J. C. and St-Onge G. (2018) Sediment provenance changes in the western arctic ocean in response to ice Rafting, Sea Level, and Oceanic Circulation Variations Since the Last Deglaciation. *Geochem. Geophys. Geosyst.* **19**, 2147–2165.
Dickinson W. R. (2004) Evolution of the North American Cordillera. *Annu. Rev. Earth Planet. Sci.* **32**, 13–45.
Dou Y., Yang S., Liu Z., Shi X., Li J., Yu H. and Berne S. (2012) Sr-Nd isotopic constraints on terrigenous sediment provenances and Kuroshio Current variability in the Okinawa Trough during the late Quaternary. *Palaeogeogr. Palaeoclimatol. Palaeoecol.* **365–366**, 38–47.
Drenzek N. J., Montluçon D. B., Yunker M. B., Macdonald R. W. and Eglinton T. I. (2007) Constraints on the origin of sedimentary organic carbon in the Beaufort Sea from coupled molecular ^{13}C and ^{14}C measurements. *Mar. Chem.* **103**, 146–162.
Druffel E. R. M., Griffin S., Glynn C. S., Benner R. and Walker B. D. (2017) Radiocarbon in dissolved organic and inorganic carbon of the Arctic Ocean. *Geophys. Res. Lett.* **44**, 2369–2376.
Dunton K. H., Goodall J. L., Schonberg S. V., Grebmeier J. M. and Maidment D. R. (2005) Multi-decadal synthesis of benthic-pelagic coupling in the western arctic: Role of cross-shelf

advective processes. *Deep Res. Part II Top. Stud. Oceanogr.* **52**, 3462–3477.

Dunton K. H., Grebmeier J. M. and Trefry J. H. (2017) Hanna Shoal: An integrative study of a High Arctic marine ecosystem in the Chukchi Sea. *Deep Res. Part II Top. Stud. Oceanogr.* **144**, 1–5.

Dürr H. H., Meybeck M. and Dürr S. H. (2005) Lithologic composition of the Earth's continental surfaces derived from a new digital map emphasizing riverine material transfer. *Global Biogeochem. Cycles* **19**, 1–23.

Eusterhues K., Rumpel C., Kleber M. and Kögel-Knabner I. (2003) Stabilisation of soil organic matter by interactions with minerals as revealed by mineral dissolution and oxidative degradation. *Org. Geochem.* **34**, 1591–1600.

Farquharson L. M., Mann D. H., Swanson D. K., Jones B. M., Buzard R. M. and Jordan J. W. (2018) Temporal and spatial variability in coastline response to declining sea-ice in northwest Alaska. *Mar. Geol.* **404**, 71–83.

Feng X., Gustafsson Holmes R. M., Vonk J. E., Van Dongen B. E., Semiletov I. P., Dudarev O. V., Yunker M. B., MacDonald R. W., Montluçon D. B. and Eglinton T. I. (2015) Multi-molecular tracers of terrestrial carbon transfer across the pan-Arctic: Comparison of hydrolyzable components with plant wax lipids and lignin phenols. *Biogeosciences* **12**, 4841–4860.

Feng X., Vonk J. E., Van Dongen B. E., Gustafsson Ö., Semiletov I. P., Dudarev O. V., Wang Z., Montluçon D. B., Wacker L. and Eglinton T. I. (2013) Differential mobilization of terrestrial carbon pools in Eurasian Arctic river basins. *Proc. Natl. Acad. Sci. U. S. A.* **110**, 14168–14173.

Fischer G. (1991) Stable carbon isotope ratios of plankton carbon and sinking organic matter from the Atlantic sector of the Southern Ocean. *Mar. Chem.* **35**, 581–596.

Folk R. L. and Ward W. C. (1957) Brazos River Bar: A Study in the Significance of grain size parameters. *J. Sediment. Petrol.* **27**, 3–26.

Forest A., Sampei M., Hattori H., Makabe R., Sasaki H., Fukuchi M., Wassmann P. and Fortier L. (2007) Particulate organic carbon fluxes on the slope of the Mackenzie Shelf (Beaufort Sea): Physical and biological forcing of shelf-basin exchanges. *J. Mar. Syst.* **68**, 39–54.

Freslon N., Bayon G., Toucanne S., Bermell S., Bollinger C., Chéron S., Etoubleau J., Germain Y., Khripounoff A., Ponzevera E. and Rouget M. L. (2014) Rare earth elements and neodymium isotopes in sedimentary organic matter. *Geochim. Cosmochim. Acta* **140**, 177–198.

Fritz M., Vonk J. E. and Lantuit H. (2017) Collapsing Arctic coastlines. *Nat. Clim. Chang.* **7**, 6–7.

Galy V., France-Lanord C. and Lartiges B. (2008) Loading and fate of particulate organic carbon from the Himalaya to the Ganga-Brahmaputra delta. *Geochim. Cosmochim. Acta* **72**, 1767–1787.

Garçon M., Chauvel C., France-Lanord C., Huyghe P. and Lavé J. Ô. (2013) Continental sedimentary processes decouple Nd and Hf isotopes. *Geochim. Cosmochim. Acta* **121**, 177–195.

Garçon M., Chauvel C., France-Lanord C., Limonta M. and Garzanti E. (2014) Which minerals control the Nd-Hf-Sr-Pb isotopic compositions of river sediments? *Chem. Geol.* **364**, 42–55.

Gardner W. D., Richardson M. J. and Mishonov A. V. (2018) Global assessment of benthic nepheloid layers and linkage with upper ocean dynamics. *Earth Planet. Sci. Lett.* **482**, 126–134.

GEOROC (2021) Geochemistry of Rocks of the Oceans and Continents. Max-Planck Institute for Chemistry, Mainz, Germany. Available at: http://georoc.mpch-mainz.gwdg.de/S [Accessed June 20, 2021].

Goericke R. and Fry B. (1994) Variations of marine plankton $\delta^{13}C$ with latitude, temperature, and dissolved CO_2 in the world ocean. *Global Biogeochem. Cycles* **8**, 85–90.

Goldstein S. L., O'Nions R. K. and Hamilton P. J. (1984) A Sm-Nd isotopic study of atmospheric dusts and particulates from major river systems. *Earth Planet. Sci. Lett.* **70**, 221–236.

Goñi M. A., O'Connor A. E., Kuzyk Z. Z., Yunker M. B., Gobeil C. and Macdonald R. W. (2013) Distribution and sources of organic matter in surface marine sediments across the North American Arctic margin. *J. Geophys. Res. Ocean.* **118**, 4017–4035.

Goñi M. A., Yunker M. B., Macdonald R. W. and Eglinton T. I. (2005) The supply and preservation of ancient and modern components of organic carbon in the Canadian Beaufort Shelf of the Arctic Ocean. *Mar. Chem.* **93**, 53–73.

Goñi M. A., Yunker M. B., MacDonald R. W. and Eglinton T. I. (2000) Distribution and sources of organic biomarkers in arctic sediments from the Mackenzie River and Beaufort Shelf. *Mar. Chem.* **71**, 23–51.

Gradinger R. (2009) Sea-ice algae: Major contributors to primary production and algal biomass in the Chukchi and Beaufort Seas during May/June 2002. *Deep Res. Part II Top. Stud. Oceanogr.* **56**, 1201–1212.

Grantz A., Hart P. E., Phillips R. L., Mc Cormick M., Perkin R. G., Jackson R., Gagnon A., Li S., Byers C. and Schwartz K. R. (1994) Preliminary results of a binational research cruise in the western arctic ocean. *Polar Geogr. Geol.* **18**, 187–210.

Grantz A., Phillips R. L. and Jones G. A. C. (1999) Holocene pelagic and turbidite sedimentation rates in the Amerasia Basin, Arctic Ocean from radiocarbon age-depth profiles in cores. In *Retrospective Collection*. Trans Tech Publications, pp. 209–222.

Grantz A., Phillips R. L., Mullen M. W., Starratt S. W., Jones G. A., Naidu A. S. and Finney B. P. (1996) Character, paleoenvironment, rate of accumulation, and evidence for seismic triggering of Holocene turbidites, Canada Abyssal Plain, Arctic Ocean. *Mar. Geol.* **133**, 51–73.

Graversen R. G., Mauritsen T., Tjernström M., Källén E. and Svensson G. (2008) Vertical structure of recent Arctic warming. *Nature* **451**, 53–56.

Grebmeier J. M., Cooper L. W., Feder H. M. and Sirenko B. I. (2006) Ecosystem dynamics of the Pacific-influenced Northern Bering and Chukchi Seas in the Amerasian Arctic. *Prog. Oceanogr.* **71**, 331–361.

Grebmeier J. M., Moore S. E., Overland J. E., Frey K. E. and Gradinger R. (2010) Biological response to recent pacific arctic sea ice retreats. *Eos (Washington. DC)* **91**, 161–162.

Grebmeier J., McRoy C. and Feder H. (1988) Pelagic-benthic coupling on the shelf of the northern Bering and Chukchi Seas. I. Food supply source and benthic bio-mass. *Mar. Ecol. Prog. Ser.* **48**, 57–67.

Grebmeier M. and Cooper L. W. (1995) Influence of the St. Lawrence Island Polynya upon the Bering Sea benthos. *J. Geophys. Res. Ocean.* **100**, 4439–4460.

Griffith D. R., McNichol A. P., Xu L., McLaughlin F. A., MacDonald R. W., Brown K. A. and Eglinton T. I. (2012) Carbon dynamics in the western Arctic Ocean: Insights from full-depth carbon isotope profiles of DIC, DOC, and POC. *Biogeosciences* **9**, 1217–1224.

Grigoriev M. N., Rachold V., Hubberten H.-W. and Schirrmeister L. (2004) Organic carbon input to the Arctic Seas trough coastal erosion. In *The organic carbon cycle in the Arctic Ocean: present and past* (eds. R. Stein and R. W. Macdonald). Springer-Verlag, Heidelberg, pp. 41–45.

Guo L. and Macdonald R. W. (2006) Source and transport of terrigenous organic matter in the upper Yukon River: Evidence

from isotope (^{13}C, ^{14}C, ^{15}N) composition of dissolved, colloidal, and particulate phases. *Global Biogeochem. Cycles* **20**, 1–12.

Guo L., Ping C. L. and Macdonald R. W. (2007) Mobilization pathways of organic carbon from permafrost to arctic rivers in a changing climate. *Geophys. Res. Lett.* **34**, 1–5.

Guo L., Semiletov I., Gustafsson Ö., Ingri J., Andersson P., Dudarev O. and White D. (2004) Characterization of Siberian Arctic coastal sediments: Implications for terrestrial organic carbon export. *Global Biogeochem. Cycles* **18**, 1–10.

Gutjahr M., Frank M., Stirling C. H., Klemm V., van de Flierdt T. and Halliday A. N. (2007) Reliable extraction of a deepwater trace metal isotope signal from Fe-Mn oxyhydroxide coatings of marine sediments. *Chem. Geol.* **242**, 351–370.

De Haas H., Van Weering T. C. E. E. and De Stigter H. (2002) Organic carbon in shelf seas: Sinks or sources, processes and products. *Cont. Shelf Res.* **22**, 691–717.

Haley B. A., Frank M., Hathorne E. and Pisias N. (2014) Biogeochemical implications from dissolved rare earth element and Nd isotope distributions in the Gulf of Alaska. *Geochim. Cosmochim. Acta* **126**, 455–474.

Haley B. A. and Polyak L. (2013) Pre-modern Arctic Ocean circulation from surface sediment neodymium isotopes. *Geophys. Res. Lett.* **40**, 893–897.

Harris P. T. and Whiteway T. (2011) Global distribution of large submarine canyons: Geomorphic differences between active and passive continental margins. *Mar. Geol.* **285**, 69–86.

Hartmann J. and Moosdorf N. (2012) The new global lithological map database GLiM: A representation of rock properties at the Earth surface. *Geochem, Geophys. Geosyst.* **13**, 1–37.

Harvey H. R. and Taylor K. A. (2017) Alkane and polycyclic aromatic hydrocarbons in sediments and benthic invertebrates of the northern Chukchi Sea. *Deep Res. Part II Top. Stud. Oceanogr.* **144**, 52–62.

Hedges J. I., Hu F. S., Devol A. H., Hartnett H. E., Tsamakis E. and Keil R. G. (1999) Sedimentary organic matter preservation: A test for selective degradation under oxic conditions. *Am. J. Sci.* **299**, 529–555.

Hedges J. I. and Keil R. G. (1995) Sedimentary organic matter preservation: an assessment and speculative synthesis. *Mar. Chem.* **49**, 81–115.

Hedges J. I., Keil R. G. and Benner R. (1997) What happens to terrestrial organic matter in the ocean? *Org. Geochem.* **27**, 195–212.

Henley S. F., Annett A. L., Ganeshram R. S., Carson D. S., Weston K., Crosta X., Tait A., Dougans J., Fallick A. E. and Clarke A. (2012) Factors influencing the stable carbon isotopic composition of suspended and sinking organic matter in the coastal Antarctic sea ice environment. *Biogeosciences* **9**, 1137–1157.

Hill V. and Cota G. (2005) Spatial patterns of primary production on the shelf, slope and basin of the Western Arctic in 2002. *Deep Sea Res. Part II Top. Stud. Oceanogr.* **52**, 3344–3354.

Hilton R. G., Galy V., Gaillardet J., Dellinger M., Bryant C., O'Regan M., Gröcke D. R., Coxall H., Bouchez J. and Calmels D. (2015) Erosion of organic carbon in the Arctic as a geological carbon dioxide sink. *Nature* **524**, 84–87.

Hobson K. A., Ambrose W. G. and Renaud P. E. (1995) Sources of primary production, benthic-pelagic coupling, and trophic relationships within the Northeast Water Polynya: insights from $\delta^{13}C$ and $\delta^{15}N$ analysis. *Mar. Ecol. Prog. Ser.* **128**, 1–10.

Holmes R. M. (2002) A circumpolar perspective on fluvial sediment flux to the Arctic ocean. *Global Biogeochem. Cycles* **16**, 1–14.

Horikawa K., Asahara Y., Yamamoto K. and Okazaki Y. (2010) Intermediate water formation in the Bering Sea during glacial periods: Evidence from neodymium isotope ratios. *Geology* **38**, 435–438.

Hwang J., Blusztajn J., Giosan L., Kim M., Manganini S. J., Montluçon D., Toole J. M. and Eglinton T. I. (2021) Lithogenic particle transport trajectories on the Northwest Atlantic Margin. *J. Geophys. Res. Ocean.* **126**, 1–11.

Hwang J., Eglinton T. I., Krishfield R. A., Manganini S. J. and Honjo S. (2008) Lateral organic carbon supply to the deep Canada Basin. *Geophys. Res. Lett.* **35**, 1–5.

Hwang J., Kim M., Manganini S. J., McIntyre C. P., Haghipour N., Park J. J., Krishfield R. A., Macdonald R. W., McLaughlin F. A. and Eglinton T. I. (2015) Temporal and spatial variability of particle transport in the deep Arctic Canada Basin. *J. Geophys. Res. Ocean.* **120**, 2784–2799.

Jacobsen S. B. and Wasserburg G. J. (1980) Sm-Nd Isotopic evolution of chondrites. *Earth Planetarv Sci. Lett.* **50**, 139–155.

Jakobsson M., Grantz A., Kristoffersen Y. and Macnab R. (2003) Physiographic provinces of the Arctic Ocean seafloor. *Bull. Geol. Soc. Am.* **115**, 1443–1455.

Jakobsson M., Mayer L., Coakley B., Dowdeswell J. A., Forbes S., Fridman B., Hodnesdal H., Noormets R., Pedersen R., Rebesco M., Schenke H. W., Zarayskaya Y., Accettella D., Armstrong A., Anderson R. M., Bienhoff P., Camerlenghi A., Church I., Edwards M., Gardner J. V., Hall J. K., Hell B., Hestvik O., Kristoffersen Y., Marcussen C., Mohammad R., Mosher D., Nghiem S. V., Pedrosa M. T., Travaglini P. G. and Weatherall P. (2012) The International Bathymetric Chart of the Arctic Ocean (IBCAO) Version 3.0. *Geophys. Res. Lett.* **39**, 1–6.

Jonell T. N., Li Y., Blusztajn J., Giosan L. and Clift P. D. (2018) Signal or noise? Isolating grain size effects on Nd and Sr isotope variability in Indus delta sediment provenance. *Chem. Geol.* **485**, 56–73.

Jones B. M., Hinkel K. M., Arp C. D. and Eisner W. R. (2008) Modern erosion rates and loss of coastal features and sites, Beaufort Sea Coastline, Alaska. *Arctic* **61**, 361–372.

Jorgenson M. T. and Brown J. (2005) Classification of the Alaskan Beaufort Sea Coast and estimation of carbon and sediment inputs from coastal erosion. *Geo-Marine Lett.* **25**, 69–80.

Kaiser K. and Guggenberger G. (2003) Mineral surfaces and soil organic matter. *Eur. J. Soil Sci.* **54**, 219–236.

Kaiser K., Mikutta R. and Guggenberger G. (2007) Increased stability of organic matter sorbed to ferrihydrite and goethite on aging. *Soil Sci. Soc. Am. J.* **71**, 711–719.

Keil R. G., Mayer L. M., Quay P. D., Richey J. E. and Hedges J. I. (1997) Loss of organic matter from riverine particles in deltas. *Geochim. Cosmochim. Acta* **61**, 1507–1511.

Keil R. G., Tsamakis E., Fuh C. B., Giddings J. C. and Hedges J. I. (1994) Mineralogical and textural controls on the organic composition of coastal marine sediments: Hydrodynamic separation using SPLITT-fractionation. *Geochim. Cosmochim. Acta* **58**, 879–893.

Kennedy M. J., Pevear D. R. and Hill R. J. (2002) Mineral surface control of organic carbon in black shale. *Science (80-)* **295**, 657–660.

Kielland K. and Bryant J. P. (1998) Moose herbivory in taiga: effects on biogeochemistry and vegetation dynamics in primary succesion. *Oikos* **82**, 377–383.

Kleber M., Sollins P. and Sutton R. (2007) A conceptual model of organo-mineral interactions in soils: Self-assembly of organic molecular fragments into zonal structures on mineral surfaces. *Biogeochemistry* **85**, 9–24.

Kuzyk Z. Z. A., Gobeil C., Goñi M. A. and Macdonald R. W. (2017) Early diagenesis and trace element accumulation in North American Arctic margin sediments. *Geochim. Cosmochim. Acta* **203**, 175–200.

Kuzyk Z. Z. A., Gobeil C. and Macdonald R. W. (2013) ^{210}Pb and ^{137}Cs in margin sediments of the Arctic Ocean: Controls on boundary scavenging. *Global Biogeochem. Cycles* **27**, 422–439.

Lalande C., Grebmeier J. M., Wassmann P., Cooper L. W., Flint M. V. and Sergeeva V. M. (2007) Export fluxes of biogenic matter in the presence and absence of seasonal sea ice cover in the Chukchi Sea. *Cont. Shelf Res.* **27**, 2051–2065.

Lantuit H., Overduin P. P., Couture N., Wetterich S., Aré F., Atkinson D., Brown J., Cherkashov G., Drozdov D., Donald Forbes L., Graves-Gaylord A., Grigoriev M., Hubberten H. W., Jordan J., Jorgenson T., Ødegård R. S., Ogorodov S., Pollard W. H., Rachold V., Sedenko S., Solomon S., Steenhuisen F., Streletskaya I. and Vasiliev A. (2012) The arctic coastal dynamics database: A new classification scheme and statistics on arctic permafrost coastlines. *Estuaries Coasts* **35**, 383–400.

Lawrence C. R., Beem-Miller J., Hoyt A. M., Monroe G., Sierra C. A., Stoner S., Heckman K., Blankinship J. C., Crow S. E., McNicol G., Trumbore S., Levine P. A., Vindušková O., Todd-Brown K., Rasmussen C., Hicks Pries C. E., Schädel C., McFarlane K., Doetterl S., Hatté C., He Y., Treat C., Harden J. W., Torn M. S., Estop-Aragonés C., Asefaw Berhe A., Keiluweit M., Della Rosa Kuhnen Á., Marin-Spiotta E., Plante A. F., Thompson A., Shi Z., Schimel J. P., Vaughn L. J. S., von Fromm S. F. and Wagai R. (2020) An open-source database for the synthesis of soil radiocarbon data: International Soil Radiocarbon Database (ISRaD) version 1.0.. *Earth Syst. Sci. Data* **12**, 61–76.

Lepore K., Moran S. B., Grebmeier J. M., Cooper L. W., Lalande C., Maslowski W., Hill V., Bates N. R., Hansell D. A., Mathis J. T. and Kelly R. P. (2007) Seasonal and interannual changes in particulate organic carbon export and deposition in the Chukchi Sea. *J. Geophys. Res.* **112**, 1–14.

Lewan M. D. (1986) Stable carbon isotopes of amorphous kerogens from Phanerozoic sedimentary rocks. *Geochim. Cosmochim. Acta* **50**, 1583–1591.

Li M., Pickart R. S., Spall M. A., Weingartner T. J., Lin P., Moore G. W. K. and Qi Y. (2019) Circulation of the Chukchi Sea shelfbreak and slope from moored timeseries. *Prog. Oceanogr.* **172**, 14–33.

Li Z., Wang X., Jin H., Ji Z., Bai Y., Chen J., Zhongqioa L., Xinyi W., Haiyan J., Zhongqiang J., Youcheng B. and Jianfang C. (2017) Variations in organic carbon loading of surface sediments from the shelf to the slope of the Chukchi Sea, Arctic Ocean. *Acta Ocean. Sin.* **36**, 3–8.

Lintern D. G., Macdonald R. W., Solomon S. M. and Jakes H. (2013) Beaufort Sea storm and resuspension modeling. *J. Mar. Syst.* **127**, 14–25.

Lowry K. E., Pickart R. S., Mills M. M., Brown Z. W., van Dijken G. L., Bates N. R. and Arrigo K. R. (2015) The influence of winter water on phytoplankton blooms in the Chukchi Sea. *Deep Res. Part II Top. Stud. Oceanogr.* **118**, 53–72.

Maccali J., Hillaire-Marcel C. and Not C. (2018) Radiogenic isotope (Nd, Pb, Sr) signatures of surface and sea ice-transported sediments from the Arctic Ocean under the present interglacial conditions. *Polar Res.* **37**, 1–13.

Macdonald R. W. and Gobeil C. (2012) Manganese Sources and Sinks in the Arctic Ocean with Reference to Periodic Enrichments in Basin Sediments. *Aquat. Geochem.* **18**, 565–591.

Macdonald R. W., Kuzyk Z. Z. A. and Johannessen S. C. (2015) The vulnerability of Arctic shelf sediments to climate change. *Environ. Rev.* **23**, 461–479.

Macdonald R. W., McLaughlin F. A. and Carmack E. C. (2002) Fresh water and its sources during the SHEBA drift in the Canada Basin of the Arctic Ocean. *Deep Res. Part I Oceanogr. Res. Pap.* **49**, 1769–1785.

Macdonald R. W., Paten D. W., Carmack E. C., Paton D. W., Carmack E. C. and Omstedt A. (1995) The freshwater budget and under-ice spreading of Mackenzie River water in the Canadian Beaufort Sea based on salinity and ^{18}O/^{16}O measurements in water and ice. *J. Geophys. Res.* **100**, 895–919.

Macdonald R. W., Solomon S. M., Cranston R. E., Welch H. E., Yunker M. B. and Gobeil C. (1998) A sediment and organic carbon budget for the Canadian beaufort shelf. *Mar. Geol.* **144**, 255–273.

Macdonald R. W., Wong C. S. and Erickson P. E. (1987) The Distribution of Nutrients in the Southeastern Beaufort Sea: Implications for Water Circulation and Primary Production. *J. Geophys. Res.* **92**, 2939–2952.

Mars J. C. and Houseknecht D. W. (2007) Quantitative remote sensing study indicates doubling of coastal erosion rate in past 50 yr along a segment of the Arctic coast of Alaska. *Geology* **35**, 583–586.

Mathis J. T., Pickart R. S., Hansell D. A., Kadko D. and Bates N. R. (2007) Eddy transport of organic carbon and nutrients from the Chukchi Shelf: Impact on the upper halocline of the western Arctic Ocean. *J. Geophys. Res. Ocean.* **112**, 1–14.

Mayer L. M. (1994a) Relationships between mineral surfaces and organic carbon concentrations in soils and sediments. *Chem. Geol.* **114**, 347–363.

Mayer L. M. (1994b) Surface area control of organic carbon accumulation in continental shelf sediments. *Geochim. Cosmochim. Acta* **58**, 1271–1284.

Mayer L. M., Schick L. L., Hardy K. R., Wagai R. and McCarthy J. (2004) Organic matter in small mesopores in sediments and soils. *Geochim. Cosmochim. Acta* **68**, 3863–3872.

McCarthy J. F., Ilavsky J., Jastrow J. D., Mayer L. M., Perfect E. and Zhuang J. (2008) Protection of organic carbon in soil microaggregates via restructuring of aggregate porosity and filling of pores with accumulating organic matter. *Geochim. Cosmochim. Acta* **72**, 4725–4744.

McClelland J. W., Holmes R. M., Dunton K. H. and Macdonald R. W. (2012) The arctic ocean estuary. *Estuaries Coasts* **35**, 353–368.

McClelland J. W., Holmes R. M., Peterson B. J., Raymond P. A., Striegl R. G., Zhulidov A. V., Zimov S. A., Tank S. E., Spencer R. G. M. M., Staples R., Gurtovaya T. Y., Griffin C. G., Zimov N., Tank S. E., Spencer R. G. M. M., Staples R., Gurtovaya T. Y. and Griffin C. G. (2016) Particulate organic carbon and nitrogen export from major Arctic rivers. *Global Biogeochem. Cycles* **30**, 629–643.

McGuire A. D., Anderson L. G., Christensen T. R., Dallimore S., Guo L., Hayes D. J., Heimann M., Lorenson T. D., Macdonald R. W. and Roulet N. (2009) Sensitivity of the carbon cycle in the Arctic to climate change. *Ecol. Monogr.* **79**, 523–555.

McGuire A. D., Chapin F. S. S., Walsh J. E. and Wirth C. (2006) Integrated regional changes in arctic climate feedbacks: Implications for the global climate system. *Annu. Rev. Environ. Resour.* **31**, 61–91.

McGuire A. D., Macdonald R. W., Schuur E. A. G., Harden J. W., Kuhry P., Hayes D. J., Christensen T. R. and Heimann M. (2010) The carbon budget of the northern cryosphere region. *Curr. Opin. Environ. Sustain.* **2**, 231–236.

McMahon R., Taveras Z., Neubert P. and Harvey H. R. (2021) Organic biomarkers and Meiofauna diversity reflect distinct carbon sources to sediments transecting the Mackenzie continental shelf. *Cont. Shelf Res.* **220**, 1–11.

Mead R. N. and Goñi M. A. (2008) Matrix protected organic matter in a river dominated margin: A possible mechanism to sequester terrestrial organic matter? *Geochim. Cosmochim. Acta* **72**, 2673–2686.

Meyer I., Davies G. R. and Stuut J. B. W. (2011) Grain size control on Sr-Nd isotope provenance studies and impact on paleoclimate reconstructions: An example from deep-sea sediments offshore NW Africa. *Geochem. Geophys. Geosyst.* **12**, 1–14.

Mikutta R., Schaumann G. E., Gildemeister D., Bonneville S., Kramer M. G., Chorover J., Chadwick O. A. and Guggenberger G. (2009) Biogeochemistry of mineral-organic associations across a long-term mineralogical soil gradient (0.3-4100 kyr), Hawaiian Islands. *Geochim. Cosmochim. Acta* **73**, 2034–2060.

Milliman J. D. and Farnsworth K. L. (2011) *River Discharge to the Coastal Ocean. A global synthesis*. Cambridge University Press, Cambride, New York, Melbourne, Madrid, Cape Town, Sinagpore, Sao Paulo, Dehli, Tokyo, Mexico City.

Millot R., Gaillardet J., Dupré B. and Allégre C. J. (2003) Northern latitude chemical weathering rates: Clues from the Mackenzie River Basin, Canada. *Geochim. Cosmochim. Acta* **67**, 1305–1329.

Morison J., Kwok R., Peralta-Ferriz C., Alkire M., Rigor I., Andersen R. and Steele M. (2012) Changing Arctic Ocean freshwater pathways. *Nature* **481**, 66–70.

Naidu A. S., Cooper L. W., Finney B. P., Macdonald R. W., Alexander C. and Semiletov I. P. (2000) Organic carbon isotope ratio ($\delta^{13}C$) of Arctic Amerasian Continental shelf sediments. *Int. J. Earth Sci.* **89**, 522–532.

Naidu A. S., Scalan R. S., Feder H. M., Goering J. J., Hameedi M. J., Parker P. L., Behrens E. W., Caughey M. E. and Jewett S. C. (1993) Stable organic carbon isotopes in sediments of the north Bering-south Chukchi seas, Alaskan-Soviet Arctic Shelf. *Cont. Shelf Res.* **13**, 669–691.

Nikolopoulos A., Pickart R. S., Fratantoni P. S., Shimada K., Torres D. J. and Jones E. P. (2009) The western Arctic boundary current at 152°W : Structure, variability, and transport. *Deep. Res. II* **56**, 1164–1181.

Norris C. E., Quideau S. A. and Oh S. W. (2016) Microbial utilization of double-labeled aspen litter in boreal aspen and spruce soils. *Soil Biol. Biochem.* **100**, 9–20.

Notz D. and Stroeve J. (2016) Observed Arctic sea-ice loss directly follows anthropogenic CO_2 emission. *Science (80-.)* **354**, 747–750.

O'Brien M. C., Macdonald R. W., Melling H. and Iseki K. (2006) Particle fluxes and geochemistry on the Canadian Beaufort Shelf: Implications for sediment transport and deposition. *Cont. Shelf Res.* **26**, 41–81.

O'Brien M. C., Melling H., Pedersen T. F. and Macdonald R. W. (2013) The role of eddies on particle flux in the Canada Basin of the Arctic Ocean. *Deep Res. Part I Oceanogr. Res. Pap.* **71**, 1–20.

Obu J., Lantuit H., Grosse G., Günther F., Sachs T., Helm V. and Fritz M. (2017) Coastal erosion and mass wasting along the Canadian Beaufort Sea based on annual airborne LiDAR elevation data. *Geomorphology* **293**, 331–346.

Oelbermann M., English M. and Schiff S. L. (2008) Evaluating carbon dynamics and microbial activity in arctic soils under warmer temperatures. *Can. J. Soil Sci.* **88**, 31–44.

Oguri K., Harada N. and Tadai O. (2012) Excess ^{210}Pb and ^{137}Cs concentrations, mass accumulation rates, and sedimentary processes on the Bering Sea continental shelf. *Deep Res. Part II Top. Stud. Oceanogr.* **61–64**, 193–204.

Osborne P. D. and Forest A. (2016) Sediment dynamics from coast to slope - Southern Canadian Beaufort Sea. *J. Coast Res.* **75**, 537–541.

Parnell A. C., Inger R., Bearhop S. and Jackson A. L. (2010) Source partitioning using stable isotopes: Coping with too much variation. *PLoS One* **5**, 1–5.

Parnell A. C., Phillips D. L., Bearhop S., Semmens B. X., Ward E. J., Moore J. W., Jackson A. L., Grey J., Kelly D. J. and Inger R. (2013) Bayesian stable isotope mixing models. *Environmetrics* **24**, 387–399.

Pebesma E. and Graeler B. (2020) gstat: Spatial and Spatio-Temporal Geostatistical Modelling, Predction and Simulation.

Peucker-Ehrenbrink B. and Miller M. W. (2003) Quantitative bedrock geology of Alaska and Canada. *Geochem. Geophys. Geosyst.* **4**, 1–10.

Pickart R. S. (2004) Shelfbreak circulation in the Alaskan Beaufort Sea: Mean structure and variability. *J. Geophys. Res. C Ocean.* **109**, 1–14.

Pickart R. S., Moore G. W. K., Mao C., Bahr F., Nobre C. and Weingartner T. J. (2016) Circulation of winter water on the Chukchi shelf in early Summer. *Deep Res. Part II Top. Stud. Oceanogr.* **130**, 56–75.

Pin C. and Santos Zalduegui J. (1997) Sequential separation of light rare-earth elements, thorium and uranium by miniaturized extraction chromatography: Application to isotopic analyses of silicate rocks. *Anal. Chim. Acta* **339**, 79–89.

Pineault S., Tremblay J. É., Gosselin M., Thomas H. and Shadwick E. (2013) The isotopic signature of particulate organic C and N in bottom ice: Key influencing factors and applications for tracing the fate of ice-algae in the Arctic Ocean. *J. Geophys. Res. Ocean.* **118**, 287–300.

Ping C. L., Michaelson G. J., Guo L., Jorgenson M. T., Kanevskiy M., Shur Y., Dou F. and Liang J. (2011) Soil carbon and material fluxes across the eroding Alaska Beaufort Sea coastline. *J. Geophys. Res. Biogeosciences* **116**, 1–12.

Pisareva M. N., Pickart R. S., Lin P., Fratantoni P. S. and Weingartner T. J. (2019) On the nature of wind-forced upwelling in Barrow Canyon. *Deep Res. Part II Top. Stud. Oceanogr.* **162**, 63–78.

Porcelli D., Andersson P. S., Baskaran M., Frank M., Björk G. and Semiletov I. (2009) The distribution of neodymium isotopes in Arctic Ocean basins. *Geochim. Cosmochim. Acta* **73**, 2645–2659.

Pourret O., Davranche M., Gruau G. and Dia A. (2007) Rare earth elements complexation with humic acid. *Chem. Geol.* **243**, 128–141.

Preston C. M., Bhatti J. S., Flanagan L. B. and Norris C. (2006) Stocks, chemistry, and sensitivity to climate change of dead organic matter along the Canadian boreal forest transect case study. *Clim. Change* **74**, 223–251.

Puig P., Palanques A. and Martín J. (2014) Contemporary sediment-transport processes in submarine canyons. *Ann. Rev. Mar. Sci.* **6**, 53–77.

R Core Team (2020) R: A language and environment for statistical computing.

Ransom B., Kim D., Kastner M. and Wainwright S. (1998) Organic matter preservation on continental slopes: importance of mineralogy and surface area. *Geochim. Cosmochim. Acta* **62**, 1329–1345.

Rearic D. M., Barnes P. W. and Reimnitz E. (1990) Bulldozing and resuspension of shallow-shelf sediment by ice keels: Implications for Arctic sediment transport trajectories. *Mar. Geol.* **91**, 133–147.

Reimer P. J., Brown T. A. and Reimer R. W. (2004) Disscusion: reporting and calibration of post-bom ^{14}C data. *Radiocarbon* **46**, 1290–1304.

Reimnitz E., McCormick M., Bischof J. and Darby D. A. (1998) Comparing sea-ice sediment load with Beaufort Sea shelf deposits; is entrainment selective? *J. Sediment. Res.* **68**, 777–787.

Rickli J., Frank M., Stichel T., Georg R. B., Vance D. and Halliday A. N. (2013) Controls on the incongruent release of

hafnium during weathering of metamorphic and sedimentary catchments. *Geochim. Cosmochim. Acta* **101**, 263–284.
Rood S. B., Kaluthota S., Philipsen L. J., Rood N. J. and Zanewich K. P. (2017) Increasing discharge from the Mackenzie River system to the Arctic Ocean. *Hydrol. Process.* **31**, 150–160.
Rothman D. H. and Forney D. C. (2007) Physical model for the decay and preservation of marine organic carbon. *Science* **316**, 1325–1329.
Ruttenberg K. C. and Goñi M. A. (1997) Phosphorus distribution, C:N: P ratios, and δ^{13}Coc in arctic, temperate, and tropical coastal sediments: tools for characterizing bulk sedimentary organic matter. *Mar. Ecol. Prog. Ser.* **139**, 123–145.
Sakshaug E. (2004) Primary and secondary production in the Arctic Sea. In *The organic carbon cycle in the Arctic Ocean* (eds. R. Stein and R. W. Macdonald). Springer, Berlin, Heidelberg, pp. 57–81.
Schell D. M. (1983) Carbon-13 and Carbon-14 abundances in alaskan aquatic organisms : delayed production from peat in arctic food webs. *Science* **219**, 1068–1071.
Schneider D. A., Backman J., Curry W. B. and Possnert G. (1996) Paleomagnetic constraints on sedimentation rates in the eastern Arctic Ocean. *Quat. Res.* **46**, 62–71.
Schreiner K. M., Bianchi T. S., Eglinton T. I., Allison M. A. and Hanna A. J. M. (2013) Sources of terrigenous inputs to surface sediments of the Colville River Delta and Simpson's Lagoon, Beaufort Sea, Alaska. *J. Geophys. Res. Biogeosci.* **118**, 808–824.
Schubert C. J. and Calvert S. E. (2001) Nitrogen and carbon isotopic composition of marine and terrestrial organic matter in Arctic Ocean sediments. *Deep Sea Res. Part I Oceanogr. Res. Pap.* **48**, 789–810.
Schulze L. M. and Pickart R. S. (2012) Seasonal variation of upwelling in the Alaskan Beaufort Sea: Impact of sea ice cover. *J. Geophys. Res. Ocean.* **117**, 1–19.
Schwab M. S., Hilton R. G., Raymond P. A., Haghipour N., Amos E., Tank S. E., Holmes R. M., Tipper E. T. and Eglinton T. I. (2020) An abrupt aging of dissolved organic carbon in large arctic rivers. *Geophys. Res. Lett.* **47**, 1–11.
Sonke J. E. and Salters V. J. M. (2006) Lanthanide-humic substances complexation. I. Experimental evidence for a lanthanide contraction effect. *Geochim. Cosmochim. Acta* **70**, 1495–1506.
Spall M. A., Pickart R. S., Fratantoni P. S. and Plueddemann A. J. (2008) Western arctic shelfbreak eddies: Formation and transport. *J. Phys. Oceanogr.* **38**, 1644–1668.
Spooner E. T. C. (1976) The strontium isotopic composition of seawater, and seawater-oceanic crust interaction. *Earth Planet. Sci. Lett.* **31**, 167–174.
Springer A. M. and McRoy C. P. (1993) The paradox of pelagic food webs in the northern Bering Sea - III. Patterns of primary production. *Cont. Shelf Res.* **13**, 575–599.
Stabeno P., Kachel N., Ladd C. and Woodgate R. (2018) Flow Patterns in the Eastern Chukchi Sea: 2010–2015. *J. Geophys. Res. Ocean.* **123**, 1177–1195.
Stein, R. and Macdonald, R. W. (eds.) (2004) *The Organic Carbon Cycle in the Arctic Ocean*. Springer, Berlin, Heidelberg.
Stolpe B., Guo L. and Shiller A. M. (2013) Binding and transport of rare earth elements by organic and iron-rich nanocolloids in alaskan rivers, as revealed by field-flow fractionation and ICP-MS. *Geochim. Cosmochim. Acta* **106**, 446–462.
Takahashi Y., Châtellier X., Hattori K. H., Kato K. and Fortin D. (2005) Adsorption of rare earth elements onto bacterial cell walls and its implication for REE sorption onto natural microbial mats. *Chem. Geol.* **219**, 53–67.
Tesi T., Semiletov I., Dudarev O., Andersson A. and Gustafsson Ö. (2016) Matrix association effects on hydrodynamic sorting and degradation of terrestrial organic matter during cross-shelf transport in the Laptev and East Siberian shelf seas. *J. Geophys. Res. Biogeosciences* **121**, 731–752.
Tessier A., Campbell P. G. C. and Bisson M. (1979) Sequential Extraction Procedure for the Speciation of Particulate Trace Metals. *Anal. Chem.* **51**, 844–851.
Thirlwall M. F. (1991) High-precision multicollector isotopic analysis of low levels of Nd as oxide. *Chem. Geol.* **94**, 13–22.
Torn M. S., Trumbore S. E., Chadwick O. A., Vitousek P. M. and Hendricks D. M. (1997) Mineral control of soil organic carbon storage and turnover. *Nature* **389**, 170–173.
Tütken T., Eisenhauer A., Wiegand B. and Hansen B. T. (2002) Glacial-interglacial cycles in Sr and Nd isotopic composition of Arctic marine sediments triggered by the Svalbard/Barents Sea ice sheet. *Mar. Geol.* **182**, 351–372.
Vance D. and Thirlwall M. (2002) An assessment of mass discrimination in MC-ICPMS using Nd isotopes. *Chem. Geol.* **185**, 227–240.
VanLaningham S., Pisias N. G., Duncan R. A. and Clift P. D. (2009) Glacial-interglacial sediment transport to the Meiji Drift, northwest Pacific Ocean: Evidence for timing of Beringian outwashing. *Earth Planet. Sci. Lett.* **277**, 64–72.
Viscosi-Shirley C., Pisias N. and Mammone K. (2003) Sediment source strength, transport pathways and accumulation patterns on the Siberian-Arctic's Chukchi and Laptev shelves. *Cont. Shelf Res.* **23**, 1201–1225.
Vonk J. E., Drenzek N. J., Hughen K. A., Stanley R. H. R., McIntyre C., Montluçon D. B., Giosan L., Southon J. R., Santos G. M., Druffel E. R. M., Andersson A. A., Sköld M. and Eglinton T. I. (2019) Temporal deconvolution of vascular plant-derived fatty acids exported from terrestrial watersheds. *Geochim. Cosmochim. Acta* **244**, 502–521.
Vonk J. E., Giosan L., Blusztajn J., Montlucon D., Graf Pannatier E., McIntyre C., Wacker L., Macdonald R. W., Yunker M. B. and Eglinton T. I. (2015) Spatial variations in geochemical characteristics of the modern Mackenzie Delta sedimentary system. *Geochim. Cosmochim. Acta* **171**, 100–120.
Vonk J. E., Sánchez-García L., Semiletov I., Dudarev O., Eglinton T., Andersson A. and Gustafsson Ö. (2010) Molecular and radiocarbon constraints on sources and degradation of terrestrial organic carbon along the Kolyma paleoriver transect. *East Siberian Sea Biogeosci.* **7**, 3153–3166.
Van der Voort T. S., Mannu U., Blattmann T. M., Bao R., Zhao M. and Eglinton T. I. (2018) Deconvolving the Fate of Carbon in Coastal Sediments. *Geophys. Res. Lett.* **45**, 4134–4142.
Wacker L., Němec M. and Bourquin J. (2010) A revolutionary graphitisation system: Fully automated, compact and simple. *Nucl. Instruments Methods Phys. Res. Sect B Beam Interact. with Mater. Atoms* **268**, 931–934.
Wagai R. and Mayer L. M. (2007) Sorptive stabilization of organic matter in soils by hydrous iron oxides. *Geochim. Cosmochim. Acta* **71**, 25–35.
Wakeham S. G. and Canuel E. A. (2016) The nature of organic carbon in density-fractionated sediments in the Sacramento-San Joaquin River Delta (California). *Biogeosciences* **13**, 567–582.
Wakeham S. G., Canuel E. A., Lerberg E. J., Mason P., Sampere T. P. and Bianchi T. S. (2009) Partitioning of organic matter in continental margin sediments among density fractions. *Mar. Chem.* **115**, 211–225.
Walsh J. J., Dieterle D. A., Maslowski W. and Whitledge T. E. (2004) Decadal shifts in biophysical forcing of Arctic marine food webs: Numerical consequences. *J. Geophys. Res. C Ocean.* **109**, 1–30.
Watanabe E., Onodera J., Harada N., Honda M. C., Kimoto K., Kikuchi T., Nishino S., Matsuno K., Yamaguchi A., Ishida A.

and Kishi M. J. () Enhanced role of eddies in the Arctic marine biological pump. *Nat. Commun.* **5**, 1–9.

Wegner C., Bennett K. E., Vernal A., De Forwick M., Fritz M., Heikkila M., Łacka M., Lantuit H., Laska M., Moskalik M., O'Regan M., Pawłowska J., Prominska A., Rachold V., Vonk J. E. and Werner K. (2015) Variability in transport of terrigenous material on the shelves and the deep Arctic Ocean during the Holocene. *Polar Res.* **34**, 1–19.

Weingartner T., Aagaard K., Woodgate R., Danielson S., Sasaki Y. and Cavalieri D. (2005) Circulation on the north central Chukchi Sea shelf. *Deep Sea Res. Part II Top. Stud. Oceanogr.* **52**, 3150–3174.

Williams W. J., Melling H., Carmack E. C. and Ingram R. G. (2008) Kugmallit Valley as a conduit for cross-shelf exchange on the Mackenzie Shelf in the Beaufort Sea. *J. Geophys. Res. Ocean.* **113**, 1–13.

Woodgate R. A. and Aagaard K. (2005) Revising the Bering Strait freshwater flux into the Arctic Ocean. *Geophys. Res. Lett.* **32**, 1–4.

Woodgate R. A., Aagaard K. and Weingartner T. J. (2005) Monthly temperature, salinity, and transport variability of the Bering Strait through flow. *Geophys. Res. Lett.* **32**, 1–4.

Xu C., Guo L., Ping C. L. and White D. M. (2009) Chemical and isotopic characterization of size-fractionated organic matter from cryoturbated tundra soils, northern Alaska. *J. Geophys. Res. Biogeosci,* **114**, 1–11.

Xu Z., Lim D., Li T., Kim S., Jung H., Wan S., Chang F. and Cai M. (2019) REEs and Sr-Nd isotope variations in a 20 ky-sediment core from the middle Okinawa Trough, East China Sea: An in-depth provenance analysis of siliciclastic components. *Mar. Geol.* **415**, 1–9.

Yamamoto-Kawai M., McLaughlin F. A., Carmack E. C., Nishino S., Shimada K. and Kurita N. (2009) Surface freshening of the Canada Basin, 2003–2007: River runoff versus sea ice meltwater. *J. Geophys. Res. Ocean.* **114**, 1–10.

Yamamoto M., Nam, II, S., Polyak L., Kobayashi D., Suzuki K., Irino T. and Shimada K. (2017) Holocene dynamics in the Bering Strait inflow to the Arctic and the Beaufort Gyre circulation based on sedimentary records from the Chukchi Sea. *Clim. Past* **13**, 1111–1127.

Yang S. Y., Jiang S. Y., Ling H. F., Xia X. P., Sun M. and Wang D. J. (2007) Sr-Nd isotopic compositions of the Changjiang sediments: Implications for tracing sediment sources. *Sci. China Ser. D Earth Sci.* **50**, 1556–1565.

Yu Y., Stern H., Fowler C., Fetterer F. and Maslanik J. (2014) Interannual variability of arctic landfast ice between 1976 and 2007. *J. Clim.* **27**, 227–243.

Yunker M. B., Backus S. M., Graf Pannatier E., Jeffries D. S. and Macdonald R. W. (2002) Sources and significance of alkane and PAH hydrocarbons in Canadian arctic rivers. *Estuar. Coast. Shelf Sci.* **55**, 1–31.

Yunker M. B. and Macdonald R. W. (1995) Composition and origins of polycyclic aromatic hydrocarbons in the Mackenzie River and on the Beaufort sea shelf. *Arctic* **48**, 118–129.

Yunker M. B., Macdonald R. W., Snowdon L. R. and Fowler B. R. (2011) Alkane and PAH biomarkers as tracers of terrigenous organic carbon in Arctic Ocean sediments. *Org. Geochem.* **42**, 1109–1146.

Zhang R., Chen M., Guo L., Gao Z., Ma Q., Cao J., Qiu Y. and Li Y. (2012) Variations in the isotopic composition of particulate organic carbon and their relation with carbon dynamics in the western Arctic Ocean. *Deep Res. Part II Top. Stud. Oceanogr.* **81–84**, 72–78.

Zhang X., Bianchi T. S., Cui X., Rosenheim B. E., Ping C. L., Hanna A. J. M., Kanevskiy M., Schreiner K. M. and Allison M. A. (2017) Permafrost Organic Carbon Mobilization From the Watershed to the Colville River Delta: Evidence From ^{14}C Ramped Pyrolysis and Lignin Biomarkers. *Geophys. Res. Lett.* **44**, 11491–11500.

Zimmermann B., Porcelli D., Frank M., Andersson P. S., Baskaran M., Lee D. C. and Halliday A. N. (2009) Hafnium isotopes in Arctic Ocean water. *Geochim. Cosmochim. Acta* **73**, 3218–3233.

Associate editor: Thomas Wagner